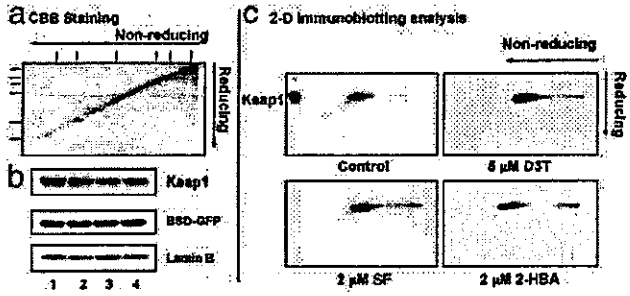


Fig. 6. Exposure to inducers causes formation of a disulfide-linked dimer of Keap1 in HEK 293 cells transfected with a construct encoding for Keap1 and GFP (normalization control). (*a*) Coomassie brilliant blue (CBB) staining of 2D SDS/PAGE of cell-free extracts. (*b*) Immunoblots of SDS/PAGE of control (lanes 1 and 2) and inducer-treated (lanes 3 and 4) cells showing (*Top*) reduced binding of the anti-Keap1 antibody for Keap1 in inducer-treated cells compared with control cells, (*Middle*) equal expression of GFP, and (*Bottom*) equal cell numbers as judged by the expression of Lamin B. (*c*) Immunoblots for Keap1 of 2D SDS/PAGE of extracts of control cells and cells exposed to inducers of three different chemical types. SF, sulforaphane; D3T, 1,2-dithiole-3-thione; 2-HBA, bis(2-hydroxybenzylidene)acetone.

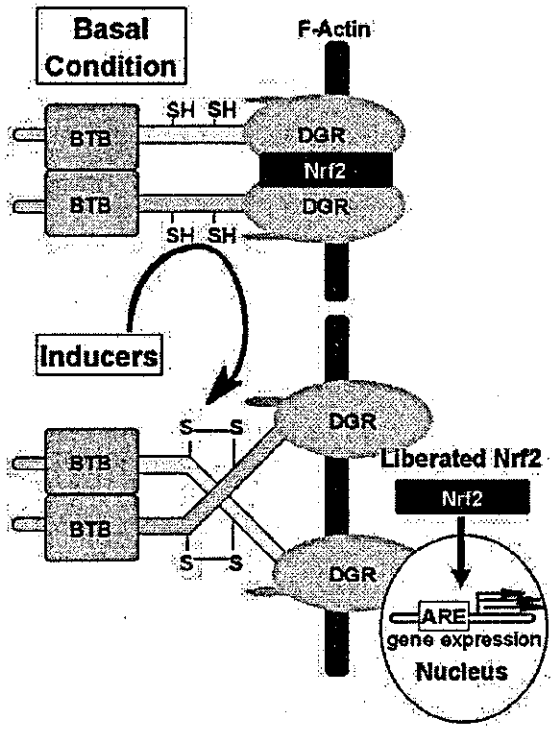


Fig. 7. Mechanism of regulation of the phase 2 response. Nrf2 (black) is retained in the cytoplasm by interaction with two molecules of Keap1, which are dimerized through their BTB domains (pink) and anchored to the actin cytoskeleton via the Kelch or DGR region (gray propeller). Inducers of the phase 2 response interact with cysteine thiol groups in the intervening region (IVR, yellow) of Keap1, causing the formation of disulfide bonds (most likely between C273 of one monomer and C288 of the other). This results in conformational change that renders Keap1 unable to bind to Nrf2, which then translocates to the nucleus. The Nrf2 in heterodimeric combination with other transcription factors such as small Maf binds to the ARE regulatory region of phase 2 genes and enhances their transcription.

phane, and 1,2-dithiole-3-thione. At the end of the exposure period, cell-free extracts were subjected to 2D SDS/PAGE (40) under nonreducing conditions in the first dimension and under reducing conditions (2-mercaptoethanol) in the second dimension. Western blot analysis was then used to localize Keap1 (Fig. 6). Only a single immunoreactive product corresponding to monomeric Keap1 was detected in uninduced cells. In contrast, the anti-Keap1 antibody recognized two products in extracts of cells treated with inducers, corresponding to a monomer and an intermolecular disulfide-linked dimer of Keap1 (Fig. 6*c*). This observation provides strong, independent evidence that reaction with inducers leads to the formation of intermolecular dimers between Keap1 subunits.

**Comparison of the Keap1/Nrf2 System with Other Genes Regulated by Oxidative Stress and Sensed by Cysteine Thiol Groups.** Although the behavior of the Keap1-Nrf2 system is in many ways unique, it resembles regulation of other proteins in which cysteine residues are modified. The prokaryotic transcription factors OxyR and SoxR are activated by oxidation, resulting in formation of intramolecular disulfide bonds in response to hydrogen peroxide and superoxide, respectively (41–44). In response to oxidants, two intramolecular disulfide bonds are formed and Zn is released from the redox-sensitive chaperone Hsp33, leading to large conformational changes which increase its affinity for protein folding intermediates, thus protecting them from oxidative damage (45, 46). Regulation of protein function can also occur by disulfide bond reduction as exemplified by activation of integrins that control cell adhesion and migration (47).

To our knowledge, the Keap1-Nrf2 system may be unique in that it depends on chemical modification of specific cysteine thiols and that the modifying agents then appear to be displaced by intermolecular sulfhydryl disulfide interchange to lead to a covalent disulfide dimer of Keap1. This eukaryotic system resembles the RsrA-SigR system from *Streptomyces coelicolor* (48–50). Both Keap1-Nrf2 and RsrA-SigR are essential components of signal transduction pathways involved in protection against oxidative stress and electrophiles by up-regulating systems that detoxify damaging agents, the Phase 2 gene products in mammals and the thioredoxin operon in *S. coelicolor*. Under basal conditions, both Keap1 and RsrA are negative regulators of the transcription factors Nrf2 and SigR, respectively. Oxidative stress or exposure to inducers disrupts the complexes, allowing the transcription factors to activate gene expression via their respective enhancer elements. Deletion of the genes encoding for Keap1 or RsrA leads to constitutive activation of the transcription factors and overexpression of the genes that are under their control, even in the absence of any stimulus. Interestingly, the IVR of Keap1 is similar in size and cysteine content to the RsrA. Individual mutations of critical cysteines of Keap1 and RsrA render them unable to repress their partner transcription factors. In both cases, this finding was completely unexpected, because the wild-type repressors are active in the reduced state and the inability to form disulfide bond(s) by mutating the participating cysteine residues is expected to lock the repressor in its constitutively active form.

These two systems present a similar paradox: (*i*) the repressors are sensors of the signal and are therefore indispensable components in the signal transduction pathway leading to induction, but if they are absent (i.e., knocked out), the same inducible genes, instead of being uninducible, are constitutively up-regulated; (*ii*) specific cysteines must be able to form disulfide bonds for repressor activity, but disulfide formation leads to release of repression, pointing out that these cysteines are not only important for inducer sensing, but also for direct interaction between the two partner (repressor/transcription factor) molecules. Their modification, for example, by disulfide bond formation, can lead to conformational changes that do not allow binding to occur. In RsrA, the critical cysteines are involved in

Zn coordination that controls the thiol-disulfide reactivity of RsrA, the Zn is expelled during oxidation with concomitant disulfide bond formation that then causes major conformational changes and does not allow binding to SigR. It is conceivable that C273 and C288 from each monomer are involved in metal coordination that, in addition to the proximity of these cysteines to basic amino acid residues, can stabilize the negative charges on the thiolate anions, lower their $pK_a$ values, and explain their unusually high reactivity.

**Summary.** These results are consistent with the model shown in Fig. 7. Under basal (reducing) conditions, Keap1 exists as a dimer in which two monomers are bound to each other, possibly by hydrophobic interactions via their BTB domains. The cysteines C273 and C288 of the intervening region are in the reduced state. In this conformation Keap1 sequesters one molecule of Nrf2 between two DGR domains in the cytoplasm and ensures its rapid turnover by targeting to the proteasome. Upon exposure to inducers, the reactive C273 and C288 residues form intermolecular disulfide bonds, thus covalently linking two monomers of Keap1. The resulting conformation separates the DGR domains, liberates Nrf2, and allows its translocation to the nucleus and enhanced expression of phase 2 genes.

We thank Philip A. Cole, Jed W. Fahey, and James T. Stivers for much perceptive advice. Robert N. Cole provided consultation and advice on the matrix-assisted laser desorption ionization/time-of-flight mass spectrometry, Osamu Ohneda helped in establishing the cell lines from the knockout mice, and Pamela Talalay provided valuable editorial consultation. These studies were supported by grants from the National Cancer Institute, Department of Health and Human Services (Grant CA 94076), the American Institute for Cancer Research (Washington, DC), and the Brassica Foundation for Cancer Chemoprotection Research (Baltimore). The AB-Mass Spectrometry Facility at the Johns Hopkins School of Medicine is funded by National Center for Research Resources Shared-Instrumentation Grant 1S10-RR14702. These studies were also supported by generous gifts from the Lewis B. and Dorothy Cullman Foundation, the Barbara Lubin Goldsmith Foundation, and the McMullan Family Fund.

1. Hayes, J. D. & McLellan, L. I. (1999) *Free Radical Res.* **31**, 273–300.
2. Talalay, P., Dinkova-Kostova, A. T. & Holtzclaw, W. D. (2003) *Adv. Enzyme Regul.* **43**, 121–134.
3. Talalay, P. (1999) *Proc. Am. Philos. Soc.* **143**, 52–72.
4. Talalay, P. (2000) *Biofactors* **12**, 5–11.
5. Ramos-Gomez, M., Kwak, M. K., Dolan, P. M., Itoh, K., Yamamoto, M., Talalay, P. & Kensler, T. W. (2001) *Proc. Natl. Acad. Sci. USA* **98**, 3410–3415.
6. Fahey, J. W., Haristoy, X., Dolan, P. M., Kensler, T. W., Scholtus, I., Stephenson, K. K., Talalay, P. & Lozniewski, A. (2002) *Proc. Natl. Acad. Sci. USA* **99**, 7610–7615.
7. Cho, H. Y., Jedlicka, A. E., Reddy, S. P., Kensler, T. W., Yamamoto, M., Zhang, L. Y. & Kleeberger, S. R. (2002) *Am. J. Respir. Cell Mol. Biol.* **26**, 175–182.
8. Henderson, C. J., Smith, A. G., Ure, J., Brown, K., Bacon, E. J. & Wolf, C. R. (1998) *Proc. Natl. Acad. Sci. USA* **95**, 5275–5280.
9. Long, D. J., Jr., Waikel, R. L., Wang, X. J., Perlaky, L., Roop, D. R. & Jaiswal, A. K. (2000) *Cancer Res.* **60**, 5913–5915.
10. Clairmont, A., Sies, H., Ramachandran, S., Lear, J. T., Smith, A. G., Bowers, B., Jones, P. W., Fryer, A. A. & Strange, R. C. (1999) *Carcinogenesis* **20**, 1235–1240.
11. Lafuente, M. J., Casterad, X., Trias, M., Ascaso, C., Molina, R., Ballesta, A., Zheng, S., Wiencke, J. K. & Lafuente, A. (2000) *Carcinogenesis* **21**, 1813–1819.
12. Smith, M. T., Wang, Y., Skibola, C. F., Slater, D. J., Lo Nigro, L., Nowell, P. C., Lange, B. J. & Felix, C. A. (2002) *Blood* **100**, 4590–4593.
13. Zhang, J., Schulz, W. A., Li, Y., Wang, R., Zotz, R., Wen, D., Siegel, D., Ross, D., Gabbert, H. E. & Sarbia, M. (2003) *Carcinogenesis* **24**, 905–909.
14. Kensler, T. W., Qian, G.-S., Chen, J.-G. & Groopman, J. D. (2003) *Nat. Rev. Cancer* **3**, 321–329.
15. Talalay, P., De Long, M. J. & Prochaska, H. J. (1988) *Proc. Natl. Acad. Sci. USA* **85**, 8261–8265.
16. Prestera, T., Zhang, Y., Spencer, S. R., Wilczak, C. A. & Talalay, P. (1993) *Adv. Enzyme Regul.* **33**, 281–296.
17. Dinkova-Kostova, A. T., Massiah, M. A., Bozak, R. E., Hicks, R. J. & Talalay, P. (2001) *Proc. Natl. Acad. Sci. USA* **98**, 3404–3409.
18. Dinkova-Kostova, A. T., Holtzclaw, W. D., Cole, R. N., Itoh, K., Wakabayashi, N., Katoh, Y., Yamamoto, M. & Talalay, P. (2002) *Proc. Natl. Acad. Sci. USA* **99**, 11908–11913.
19. Kang, M.-I., Kobayashi, A., Wakabayashi, N., Kim, S.-G. & Yamamoto, M. (2004) *Proc. Natl. Acad. Sci. USA* **101**, 2046–2051.
20. Levonen, A.-L., Landar, A., Ramachandran, A., Ceaser, E. K., Dickinson, D. A., Zanoni, G., Morrow, J. D. & Darley-Usmar, V. M. (2003) *Biochem. J.*, in press.
21. Zhang, D. D. & Hannik, M. (2003) *Mol. Cell. Biol.* **23**, 8137–8151.
22. Hayes, J. D. & McMahon, M. (2001) *Cancer Lett.* **174**, 103–113.
23. Nguyen, T., Sherratt, P. J. & Pickett, C. B. (2003) *Annu. Rev. Pharmocol. Toxicol.* **43**, 233–260.
24. Chui, D. H., Tang, W. & Orkin, S. H. (1995) *Biochem. Biophys. Res. Commun.* **209**, 40–46.
25. Itoh, K., Chiba, T., Takahashi, S., Ishii, T., Igarashi, K., Katoh, Y., Oyake, T., Hayashi, N., Satoh, K., Hatayama, I., *et al.* (1997) *Biochem. Biophys. Res. Commun.* **236**, 313–322.
26. Venugopal, R. & Jaiswal, A. K. (1996) *Proc. Natl. Acad. Sci. USA* **93**, 14960–14965.
27. Itoh, K., Wakabayashi, N., Katoh, Y., Ishii, T., Igarashi, K., Engel, J. D. & Yamamoto, M. (1999) *Genes Dev.* **13**, 76–86.
28. Itoh, K., Wakabayashi, N., Katoh, Y., Ishii, T., O'Connor, T. & Yamamoto, M. (2003) *Genes Cells.* **8**, 379–391.
29. McMahon, M., Itoh, K., Yamamoto, M. & Hayes, J. D. (2003) *J. Biol. Chem.* **278**, 21592–21600.
30. Nguyen, T., Sherratt, P. J., Huang, H. C., Yang, C. S. & Pickett, C. B. (2003) *J. Biol. Chem.* **278**, 4536–4541.
31. Sekhar, K. R., Yan, X. X. & Freeman, M. L. (2002) *Oncogene* **21**, 6829–6834.
32. Stewart, D., Killeen, E., Naquin, R., Alam, S. & Alam, J. (2003) *J. Biol. Chem.* **278**, 2396–2402.
33. Zipper, L. M. & Mulcahy, R. T. (2002) *J. Biol. Chem.* **277**, 36544–36552.
34. Prag, S. & Adams, J. C. (2003) *BMC Bioinformatics* **4**, 42.
35. Hogan, B., Constantini, F. & Lacy, Y. (1986) *Manupulating the Mouse Embryo: A Laboratory Manual* (Cold Spring Harbor Lab. Press, Plainview, NY).
36. Wakabayashi, N., Itoh, K., Wakabayashi, J., Motohashi, H., Noda, S., Takahashi, S., Imakado, S., Kotsuji, T., Otsuka, F., Roop, D. R., *et al.* (2003) *Nat. Genet.* **35**, 238–245.
37. Zhang, Y. & Callaway, E. C. (2002) *Biochem J.* **364**, 301–307.
38. Favreau, L. V.& Pickett, C. B. (1995) *J. Biol. Chem.* **270**, 24468–24474.
39. Snyder, G. H., Cennerazzo, M. J., Karalis, A. J. & Field, D. (1981) *Biochemistry* **20**, 6509–6519.
40. Hynes, R. O. & Destree, A. (1977) *Proc. Natl. Acad. Sci. USA* **74**, 2855–2859.
41. Zheng, M., Aslund, F. & Storz, G. (1988) *Science* **279**, 1718–1721.
42. Zheng, M. & Storz, G. (2000) *Biochem. Pharmacol.* **59**, 1–6.
43. Sun, Y. & Oberley, L. W. (1996) *Free Radical Biol. Med.* **21**, 335–348.
44. Georgiou, G. (2002) *Cell* **111**, 607–610.
45. Graumann, J., Lilie, H., Tang, X., Tucker, K. A., Hoffmann, J. H., Vijayalakshmi, J., Saper, M., Bardwell, J. C. & Jakob, U. (2001) *Structure (Cambridge, Mass.)* **9**, 377–387.
46. Linke, K. & Jakob, U. (2003) *Antioxid. Redox Signal.* **5**, 425–434.
47. Yan, B. & Smith, S. W. (2001) *Biochemistry* **40**, 8861–8867.
48. Kang, J.-G., Paget, M. S. B., Seok, Y.-J., Hahn, M.-Y., Bae, J.-B., Hahn, J.-S., Kleanthous, C., Buttner, M. J. & Roe, J.-H. (1999) *EMBO J.* **18**, 4292–4298.
49. Paget, M. S., Bae, J. B., Hahn, M. Y., Li, W., Kleanthous, C., Roe, J. H. & Buttner, M. J. (2001) *Mol. Microbiol.* **39**, 1036–1047.
50. Li, W., Bottrill, A. R., Bibb, M. J., Buttner, M. J., Paget, M. S. & Kleanthous, C. (2003) *J. Mol. Biol.* **333**, 461–472.

# Scaffolding of Keap1 to the actin cytoskeleton controls the function of Nrf2 as key regulator of cytoprotective phase 2 genes

Moon-Il Kang*†, Akira Kobayashi*†, Nobunao Wakabayashi*, Sang-Geon Kim‡, and Masayuki Yamamoto*†§

*Center for Tsukuba Advanced Research Alliance and †Japan Science and Technology Agency–Exploratory Research for Advanced Technology Environmental Response Project, University of Tsukuba, 1-1-1 Tennoudai, Tsukuba 305-8575, Japan; and ‡National Research Laboratory, College of Pharmacy and Research Institute of Pharmaceutical Sciences, Seoul National University, Seoul 151-742, Korea

Communicated by Paul Talalay, Johns Hopkins University School of Medicine, Baltimore, MD, December 16, 2003 (received for review November 8, 2003)

**Transcription factor Nrf2 regulates basal and inducible expression of phase 2 proteins that protect animal cells against the toxic effects of electrophiles and oxidants. Under basal conditions, Nrf2 is sequestered in the cytoplasm by Keap1, a multidomain, cysteine-rich protein that is bound to the actin cytoskeleton. Keap1 acts both as a repressor of the Nrf2 transactivation and as a sensor of phase 2 inducers. Electrophiles and oxidants disrupt the Keap1–Nrf2 complex, resulting in nuclear accumulation of Nrf2, where it enhances the transcription of phase 2 genes via a common upstream regulatory element, the antioxidant response element. Reporter cotransfection–transactivation analyses with a series of Keap1 deletion mutants revealed that in the absence of the double glycine repeat domain Keap1 does not bind to Nrf2. In addition, deletion of either the intervening region or the C-terminal region also abolished the ability of Keap1 to sequester Nrf2, indicating that all of these domains contribute to the repressor activity of Keap1. Immunocytochemical and immunoprecipitation analyses demonstrated that Keap1 associates with actin filaments in the cytoplasm through its double glycine repeat domain. Importantly, disruption of the actin cytoskeleton promotes nuclear entry of an Nrf2 reporter protein. The actin cytoskeleton therefore provides scaffolding that is essential for the function of Keap1, which is the sensor for oxidative and electrophilic stress.**

Oxidative and electrophilic stresses provoke physiological responses that induce the expression of various cytoprotective genes (1). Recently, the transcription factor Nrf2 (2) or ECH (3) was identified as the major regulator of the cytoprotective genes encoding phase 2 detoxication and antioxidant enzymes (4, 5). Nrf2, a basic region–leucine zipper (b-Zip) transcription factor (6) contains the N-terminal Neh2 domain, which is conserved between human Nrf2 (2) and chicken ECH (3). Biochemical analyses further revealed that the Neh2 domain serves as a negative regulatory domain of Nrf2 transcriptional activity, and we subsequently isolated a protein, Keap1, as an Neh2-associated protein (7).

Keap1 shares close similarity with *Drosophila* Kelch protein, which is essential for the formation of actin-rich intracellular bridges termed ring canals (8). These proteins have two common characteristic domains, i.e., the BTB (Broad complex, Tramtrack, and Bric a Brac)/POZ (poxvirus and zinc finger) and double glycine repeat (DGR or Kelch repeats) domains at the N- and C-terminal regions (NTR and CTR), respectively. The BTB domain of Keap1 has been examined in a transfection assay and was shown to be important for Keap1 function (9). The DGR domain comprises six repeats of the Kelch motif, and according to the x-ray structural analysis of galactose oxidase, which is a protein containing a Kelch motif, Kelch repeats form $\beta$-propeller structures (10). Importantly, many Kelch-related proteins colocalize with actin filaments through the Kelch repeats, suggesting a biological role of the DGR domain in the regulation and maintenance of the cytoskeleton (11, 12).

The association of Nrf2 with Keap1 has been examined (7). In the absence of electrophiles or oxidants, Nrf2 localizes in the cytoplasm in association with Keap1. On exposure to these inducers, however, Keap1 liberates Nrf2, allowing it to translocate to the nucleus and transactivate cytoprotective genes. Germline Nrf2-deficient mice have significantly reduced inducible and/or basal level expression of phase 2 and antioxidant enzymes compared with wild-type mice (4, 5). Deficient expression of cytoprotective enzymes renders mice highly sensitive to carcinogens and oxidative stresses, demonstrating that Nrf2 plays major roles in the defense systems against chemical carcinogenesis and acute drug intoxication (reviewed in refs. 1 and 13).

We also generated germline Keap1-deficient mice (14). Although homozygous *Keap1* mutant newborns appeared normal, they all died within 3 weeks after birth. Detailed postmortem analyses revealed severe hyperkeratosis in the esophagus and forestomach of these mutants. We found that the Keap1–Nrf2 pathway also regulates a subset of genes induced in squamous cell epithelia in response to mechanical stress. Importantly, all of the Keap1-dependent phenotypes were reversed in *Keap1–Nrf2* combined null-mutant mice, indicating that the Keap1 deficiency caused Nrf2 to accumulate constitutively accumulate in the nucleus. These results thus establish that the Keap1–Nrf2 system is an essential regulatory pathway that controls the cellular response to oxidative and xenobiotic stresses.

These *in vivo* examinations led us to address the next important question: how signals from oxidants and electrophiles are transmitted to the Keap1–Nrf2 system. Because the only common chemical property of phase 2 inducers is their ability to react with sulfhydryl groups, it has been proposed that the inducers may react with cysteine residues of a sensor protein (15). Indeed, Keap1 contains 25 cysteine residues, some of which have the characteristics of reactive cysteine. Phase 2 inducers react with sulfhydryl groups of Keap1, resulting in the disruption of the Keap1–Nrf2 complex (23). Hence, we envisage that Keap1 may function as one of the stress sensors in eukaryotes. Here, we describe the molecular mechanisms whereby Keap1 regulates Nrf2 activity under unstressed conditions. We identified five domains of Keap1 that may have discrete functions. These domains are referred to as N-terminal region (NTR), BTB, intervening region (IVR), DGR, and C-terminal region (CTR). In closer structure–function analyses of these domains, we found that Keap1 interacts with the actin filaments through DGR and that this interaction is crucial for Keap1 activity. We also found

Abbreviations: ARE, antioxidant response element; BTB, Broad complex, Tramtrack, and Bric-a-Brac; CTR, C-terminal region; DGR, double glycine repeat; IVR, intervening region; NTR, N-terminal region.

§To whom correspondence should be addressed at: Center for Tsukuba Advanced Research Alliance, University of Tsukuba, 1-1-1 Tennoudai, Tsukuba 305-8575, Japan. E-mail: masi@tara.tsukuba.ac.jp.





www.pnas.org/cgi/doi/10.1073/pnas.0308347100

that both IVR and CTR are essential for Keap1 to retain Nrf2 in the cytoplasm. Taken together, these data demonstrate that the Keap1–Nrf2 system provides a unique biological regulatory mechanism, formed through interaction with the actin filament network.

## Experimental Procedures

**Plasmid Construction.** Full-length mouse Keap1 cDNA was subcloned into pcDNA3 (Invitrogen) vector (pcDNA-mKeap1). Keap1 deletion mutants were generated by inserting appropriate PCR-amplified cDNA fragments into the pcDNA3 vector. Information on the primers is available on request. These mutants were named ΔNTR (amino acids 1–60 deleted), ΔBTB (amino acids 61–179 deleted), ΔIVR (amino acids 192–308 deleted), ΔDGR (amino acids 315–598 deleted), and ΔCTR (amino acids 599–624 deleted). Structures of all constructs were verified by DNA sequencing.

**Transfection Experiments and Luciferase Assay.** Transfection experiments were performed as described (7) by using Lipofectamine plus reagents (Invitrogen). Luciferase assay was performed by using the Dual-Luciferase reporter assay system (Promega). Expression plasmids of Keap1 deletion mutants and Nrf2 were transfected into NIH 3T3 cells along with pNQO1 (nicotinamide quinone oxidoreductase 1)-ARE (antioxidant response element) reporter plasmid and pRL-TK as a control. pNQO1-ARE plasmid contains a single ARE and was used to measure the transactivation activity of Nrf2.

**Laser Confocal Scanning Microscopy.** A mouse Keap1 cDNA fragment was inserted into pCAGGS vector (pCAGGS-mKeap1; ref. 17). The resultant plasmid was injected into fertilized eggs and mouse embryonic fibroblasts (MEF) were prepared from transgene-positive 14.5-day-old embryos. Subcellular localization of Keap1 and actin was examined by immunohistochemical staining with laser confocal microscope (Leica). Anti-Keap1 antibodies were raised in rabbits by a standard method by using oligopeptides against the N and C termini of Keap1 individually.

**Immunohistochemical Staining.** Expression plasmids of Neh2-GFP and Keap1 deletion mutants were transfected into NIH 3T3 cells grown on slides. Cells were washed and fixed 36 h after transfection as described (7). Actin filament disruption experiments were modified from previous methods (18–21). In brief, cells were incubated with cytochalasin B (6 μM), swinholide A (50 nM), or colchicines (1 μM) for several periods of time as described in the figure legends. Cells were washed with PBS, blocked with 2% goat serum, and treated with anti-Keap1 antibody (100-fold dilution). Cells were then treated with goat anti-rabbit IgG conjugated with tetramethylrhodamine B isothiocyanate (TRITC, Zymed), 4′,6-diamidino-2-phenylindole (DAPI, 200 ng/ml), and Texas red-X phalloidin (200 units/ml, Molecular Probes). After washing with PBS, a drop of fluorescent mounting medium (DAKO) was placed on the slides.

**Immunoprecipitation Analysis.** 293T cells expressing Keap1 deletion mutants and Flag-Nrf2 were grown on culture dishes. Cells were harvested with Harlow buffer (50 mM Tris·HCl, pH 7.5/1% Nonidet P-40/20 mM EDTA/50 mM NaF) supplemented with protease inhibitors (Roche Diagnostics). Cell extracts were first cleared with protein G Sepharose and incubated with ANTI-FLAG M2 affinity gel (Sigma) or anti-actin (C-2) mouse monoclonal IgG (Santa Cruz Biotechnology) bound to protein G Sepharose. The immunocomplexes were washed five times with Harlow solution and subjected to immunoblot analysis.

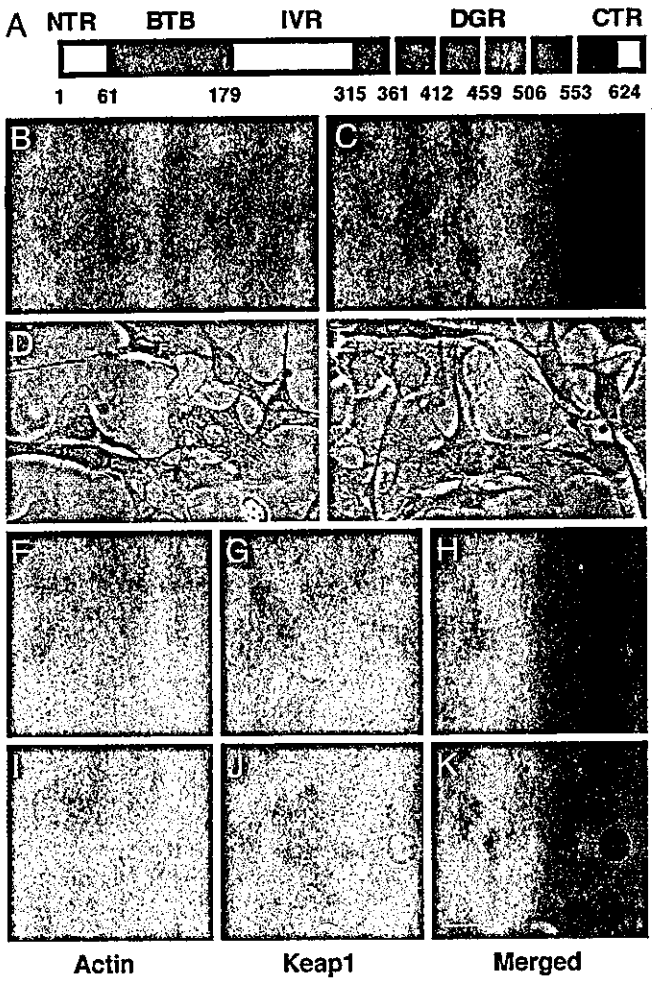


Fig. 1. Keap1 colocalizes with actin filaments in the cytoplasm. (*A*) Schematic presentation of Keap1 based on Swiss-Prot, using the Sanger Center Database. We assigned five domains within Keap1: NTR, BTB, IVR, DGR, and CTR. (*B–E*) Cytoplasmic localization of Keap1 in NIH 3T3 cells. Keap1 was expressed in NIH 3T3 cells, and subcellular localization of Keap1 was detected immunohistochemically by two anti-Keap1 antibodies against the N- and C-terminal ends of Keap1 (*B* and *C*, respectively). Bright-field microscopic images for *B* and *C* are shown in *D* and *E*, respectively. (*F–K*) colocalization of Keap1 and actin filaments in MEF derived from transgenic mouse embryos expressing Keap1. Subcellular localization of actin filaments (*F* and *I*) and Keap1 (*G* and *J*) are visualized by staining with phalloidin conjugated with Texas red and anti-Keap1 antibody, respectively. *H* and *K* show merged signals. Fluorescence was recorded by confocal microscopy. (Scale bar, 40 μm.)

## Results

**Keap1 Functions as an Actin-Binding Protein.** To clarify the molecular mechanisms of Keap1 function, we first investigated the functional domains of Keap1. Comparison of the amino acid sequences of mouse, rat, and human (KIAA0132) Keap1 proteins shows that their sequences are highly conserved (>94%) among these species (data not shown). Pfam database (q9z2x8, mouse Keap1) analyses indicate that Keap1 protein consists of five characteristic domains: NTR, BTB/POZ, IVR, DGR, and CTR (Fig. 1*A*). The DGR structure also exists in other Kelch-related proteins, and some of them, such as Mayven (22), have been reported to interact with actin filaments through DGR. These data led us to examine whether Keap1 might act as an actin-binding protein.

We examined the colocalization of Keap1 with actin filaments in the cytoplasm. We raised two anti-Keap1 antibodies, which

recognize either the N-terminal or the C-terminal end regions of Keap1. Keap1 expression plasmid was transfected into NIH 3T3 cells, and the subcellular localization of Keap1 was monitored by immunocytochemical staining with anti-Keap1 antibodies. Both anti-N terminus antibody (Fig. 1 *B* and *D*) and anti-C terminus antibody (*C* and *E*) recognized Keap1 as a cytoplasmic factor. The localization of the signals suggests a fiber-based distribution of Keap1.

The subcellular localization of Keap1 was examined by confocal microscopy. Because the expression level of endogenous Keap1 was below the detection limit of the antibodies, for this analysis we prepared transgenic mice that express Keap1 at relatively high levels under the regulation of the CAGGS promoter (17). We assumed that overexpression of Keap1 in transgenic mouse embryos would reflect the physiological localization of Keap1 more closely than overexpression in cultured cells. Overexpression of Keap1 in transgenic mice did not affect the development or growth of the mice (data not shown). Immunostaining of mouse embryonic fibroblasts (MEF) derived from the transgenic embryos with the mixture of anti-Keap1 antibodies is shown in Fig. 1 (*F–K*) along with the staining of actin filaments with phalloidin conjugated with Texas red. Keap1 was localized in the perinuclear region and showed a fibrous pattern (*G* and *J*); and expression of Keap1 appeared to overlap that of the actin filaments (*F* and *I*). When we merged the two staining patterns, they overlapped markedly (*H* and *K*). The overlapping image (yellow) is more pronounced in the perinuclear region than in the region beneath the plasma membrane. Thus, these data suggest that Keap1 may bind directly to the actin filaments or cytoskeleton in the cytoplasm.

**Direct Association of Keap1 with Actin Through DGR.** To address whether Keap1 and actin filaments interact directly, we performed an immunoprecipitation analysis by using whole-cell extracts of 293T cells expressing a series of Keap1 deletion mutants (Fig. 2*A*). Precipitates obtained by anti-actin antibody were subjected to immunoblot analysis with anti-Keap1 antibodies. As shown in Fig. 2*B*, Keap1 was detected in the complex precipitated by the anti-actin antibody (*Upper*, lane 1), indicating that Keap1 and actin filaments interact directly.

To identify the surface of Keap1 interacting with actin, we carried out similar analyses with a series of Keap1 deletion mutants. The anti-actin antibody precipitated ΔNTR, ΔBTB, ΔIVR, and ΔCTR mutant proteins (Fig. 2*B*, lanes 2–5) but not the ΔDGR mutant protein (lane 7). Immunoblotting analysis with the anti-Keap1 antibodies indicated the presence of ΔDGR Keap1 protein as well as other mutant proteins in the whole-cell extracts (Fig. 2*B Lower*). These results demonstrate that DGR is the domain primarily responsible for the interaction of Keap1 with actin filaments.

**Keap1 Requires Actin Filaments as Scaffolding.** The results described above indicate that Keap1 retains Nrf2 in the cytoplasm under unstressed conditions. To elucidate whether the Keap1 activity requires actin filaments as scaffolding, we disrupted the actin cytoskeleton and examined the effect on the subcellular localization of Nrf2. NIH 3T3 cells were treated with cytochalasin B or swinholide A, which inhibit polymerization of actin filaments, and stained with phalloidin. Because prolonged treatment of NIH 3T3 cells (>12 h) with these compounds induced cell death (data not shown), we treated the cells with these reagents for <3 h and analyzed the effects. As a negative control, we also used colchicine, a specific inhibitor of microtubule polymerization. As shown in Fig. 3, treatment of NIH 3T3 cells with cytochalasin B or swinholide A disrupted the actin filament network effectively within 3 h (Fig. 3 *A–C*), whereas that with colchicine did not (Fig. 3*D*).

We then examined the effect of actin disruption on localization of Neh2-GFP containing GFP fused to the Neh2 domain in NIH 3T3 cells. Because we previously established that the Neh2 domain is the interactive interface of Nrf2 with Keap1 (7), we used this fusion protein as a reporter for the expression site of Nrf2. The subcellular localization of Neh2-GFP and Keap1 were monitored by the green fluorescence of GFP and immunostaining with anti-Keap1 antibodies, respectively. Whereas Neh2-GFP was localized exclusively in the cytoplasm in the presence of Keap1 (Fig. 3 *E* and *F*, 0 h), treatment with cytochalasin B resulted in an ≈5-fold increase in nuclear translocation of Neh2-GFP within 1 h. Additional incubation of the cells for 2 and 3 h with these reagents did not further enhance the entry of Neh2-GFP into the nucleus. The results are summarized in Fig. 3*F*. Subcellular localization of Neh2-GFP and Keap1 after treatment with swinholide A showed essentially similar profiles (Fig. 3*F*). In contrast, treatment with colchicine did not affect significantly the subcellular localization of Neh2-GFP (Fig. 3*F*, black bars). These results establish that disruption of the actin filament network releases Neh2-GFP from Keap1, resulting in entry of Neh2-GFP into the nucleus, thereby supporting our contention that Keap1 requires the actin cytoskeleton as a scaffold to sequester Nrf2 efficiently in the cytoplasm.

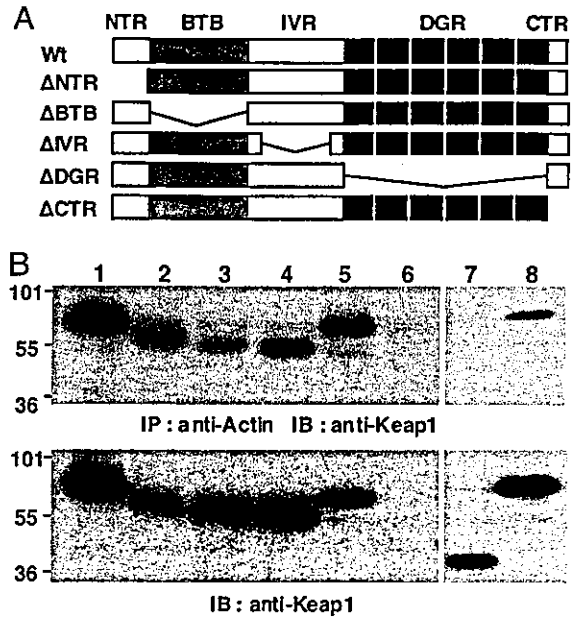


Fig. 2. Keap1 interacts with actin filaments through the DGR domain. (*A*) Schematic presentation of the structure of Keap1 deletion mutants. (*B*) Immunoprecipitation with whole-cell extracts of 293T cells expressing deletion mutants of Keap1. Immunoprecipitates (IP) obtained by anti-actin antibody were subjected to immunoblot analysis (IB) with anti-Keap1 antibody (*Upper*). The expression level of Keap1 deletion mutants was verified by immunoblot analysis (*Lower*). Analysis with wild-type Keap1-transfected cell lysates (lanes 1 and 8) as well as cell lysates transfected with Keap1 mutant ΔNTR (lane 2), ΔBTB (lane 3), ΔIVR (lane 4), ΔCTR (lane 5), and ΔDGR (lane 7) are shown. Lane 6 is loaded with cell extract expressing Nrf2 but not Keap1. Two anti-Keap1 antibodies were used: one against CTR (lanes 1–6) and the other against NTR (lanes 7 and 8).

**Identification of a New Function of CTR.** We examined the domain function of Keap1 further by expressing Keap1 deletion mutants (see Fig. 2*A*) and Neh2-GFP. Immunocytochemical staining with anti-Keap1 antibodies showed that all deletion mutants of Keap1 were localized in the cytoplasm (Fig. 4). In addition, wild-type Keap1 as well as ΔNTR, ΔBTB, and ΔIVR mutants localized Neh2-GFP exclusively in the cytoplasm, whereas ΔDGR and ΔCTR mutants of Keap1 did not. These results

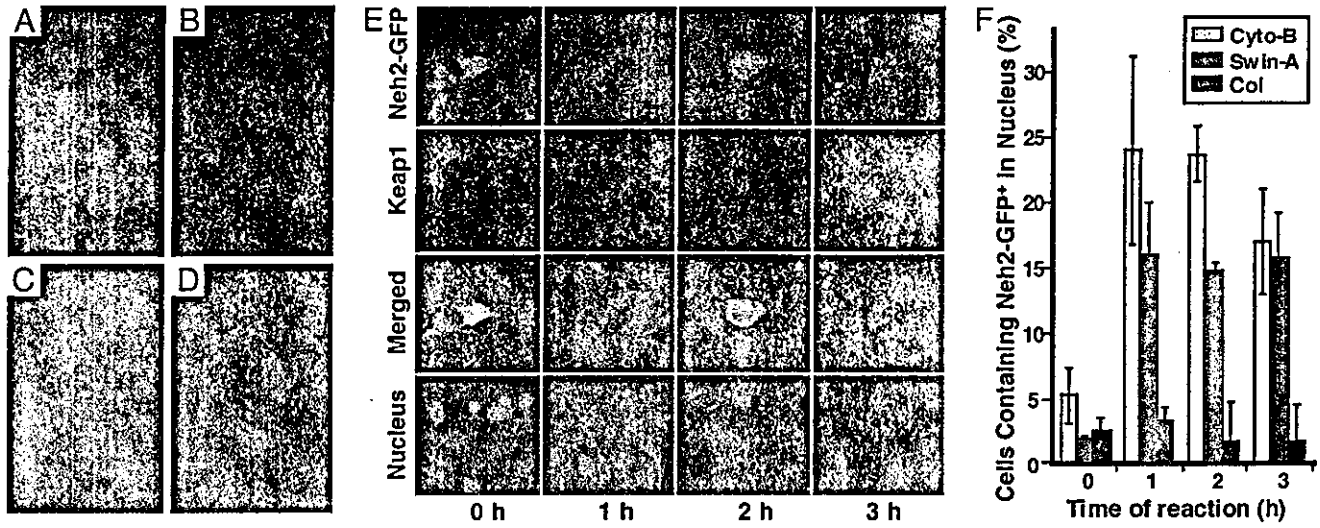


**Fig. 3.** Disruption of actin filaments triggers nuclear transport of Neh2-GFP. (*A*) NIH 3T3 cells were stained with phalloidin conjugated with Texas red and 4′,6-diamidino-2-phenylindole (DAPI) after addition of DMSO (*A*; a vehicle control) or cytoskeletal filament disruptors, cytochalasin B (*B*), swinholide A (*C*), or colchicine (*D*). (*E*) subcellular localization of Neh2-GFP and Keap1 after treatment with cytochalasin B. Cells ($4 \times 10^3$) were transfected with expression plasmids of Keap1 (0.2 $\mu$g) and Neh2-GFP, a reporter protein of Nrf2 (0.8 $\mu$g). The latter is a fusion protein of Neh2 domain and GFP. Localization of these proteins was examined by fluorescence microscopy with use of GFP fluorescence and anti-Keap1 antibody, respectively (first and second rows). Merged images of Neh2-GFP and Keap1 signals are shown in the third row. Nuclei are shown with DAPI staining (fourth row). (Original magnification, ×400.) (*F*) nuclear transport of Neh2-GFP 3 h after the addition of cytochalasin B (Cyto-B), swinholide A (Swin-A), and colchicine (Col). Shown is the percentage of cells expressing Neh2-GFP in nucleus among the total transfected cells. The average and standard errors represent three independent transfection experiments.

suggest that in addition to DGR, CTR is also critical for Keap1 to retain Nrf2 in the cytoplasm.

**DGR, but Not CTR, Directly Associates with Nrf2.** We examined the direct interaction of each domain of Keap1 with Nrf2 by immunoprecipitation. Whole-cell extracts of 293T cells expressing a series of Keap1 deletion mutants and Flag-tagged Nrf2 were subjected to immunoprecipitation analysis by using anti-Flag antibody and then immunoblot analysis with anti-Keap1 antibodies. Consistent with the results in Fig. 4, deletion of DGR completely abolished the association of Keap1 with Nrf2 (Fig. 5*A*, lane 8). The amount of Nrf2 in the whole-cell extracts was monitored by immunoblot analysis with anti-Nrf2 antibody (Fig. 5*B*). Thus, DGR appears to be indispensable for interaction with both Nrf2 and actin filaments.

Surprisingly, the ΔCTR mutant interacted with Nrf2 in this immunoprecipitation analysis (Fig. 5*A*, lane 7), although this mutant did not retain Neh2-GFP in the cytoplasm (Fig. 4, ΔCTR). One plausible explanation for this discrepancy is that the CTR domain may modulate the conformation of DGR *in vivo* and thus regulate the interaction between Keap1 and Nrf2.



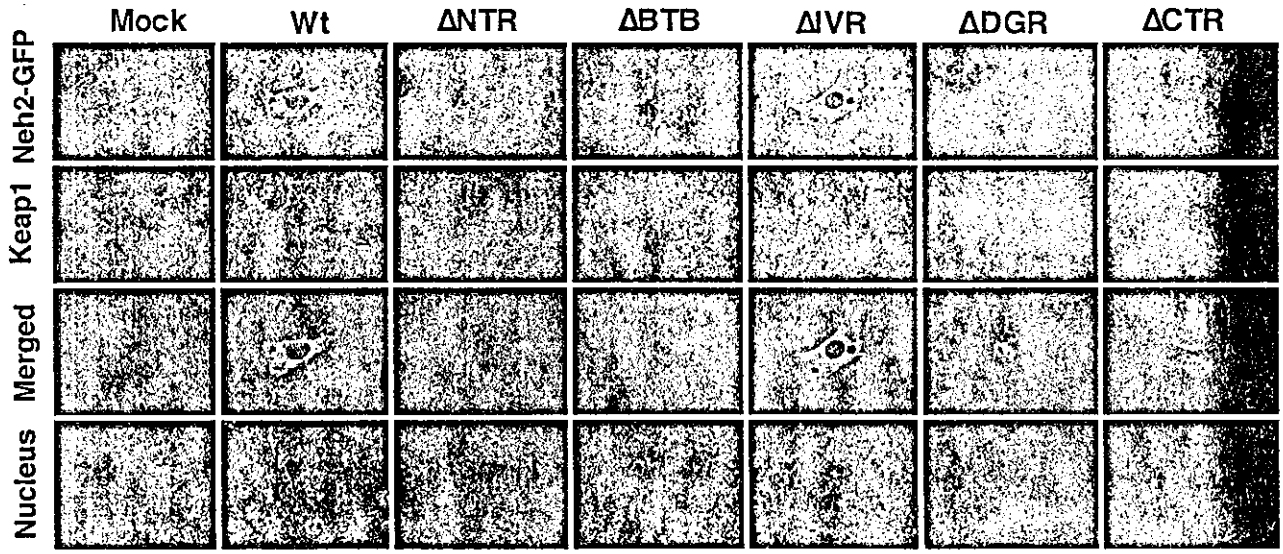


**Fig. 4.** CTR contributes to Keap1 activity retaining Neh2-GFP in cytoplasm. Subcellular localization of Neh2-GFP was examined in the presence of Keap1 deletion mutants. Transfection was performed as described in the legend to Fig. 3. Localization of Neh2-GFP and Keap1 mutant proteins was examined by fluorescence microscopy (first and second rows). Merged signals of both Neh2-GFP and Keap1 are shown in the third row. Nuclei are shown with DAPI staining (shown as Nucleus; fourth row). (Original magnification, ×400.)

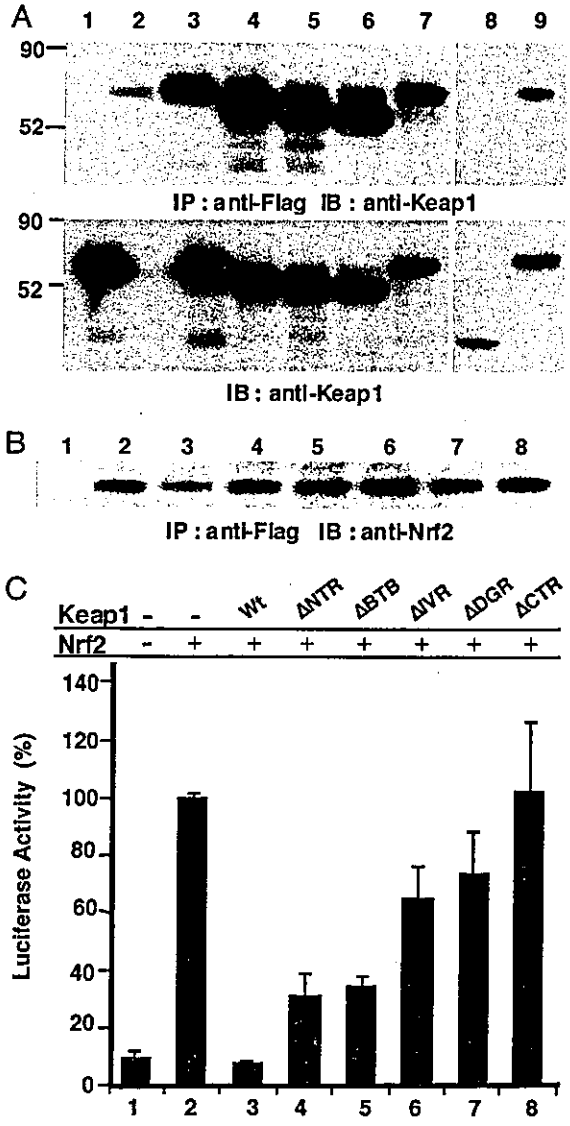


Fig. 5. IVR and CTR are both essential for Keap1 repression of Nrf2. (*A*) DGR of Keap1 directly associates with Nrf2. Whole-cell extracts prepared from 293T cells cotransfected with expression plasmids of various Keap1 deletion mutants (2 $\mu$g) and Flag-tagged Nrf2 (2 $\mu$g) were subjected to immunoprecipitation (IP). Immunoprecipitates obtained by anti-Flag antibody were subjected to immunoblot analysis (IB) with anti-Keap1 antibodies (*Upper*). The expression level of Keap1 deletion mutants was verified by immunoblot analysis (*Lower*). Analysis of cell lysates cotransfected with Nrf2 and wild-type Keap1 (lanes 3 and 9) as well as cell lysates cotransfected with Nrf2 and Keap1 ΔNTR (lane 4), ΔBTB (lane 5), ΔIVR (lane 6), ΔCTR (lane 7), or ΔDGR (lane 8) mutants are shown. Lane 1 is loaded with cell extract expressing only Keap1, and lane 2 is loaded with Nrf2 only. Anti-Keap1 CTR antibody was used in lanes 1–7, and anti-Keap1 NTR antibody was used for lanes 8 and 9. (*B*) Expression level of Nrf2 in immunoprecipitates was monitored by immunoblot analysis with anti-Nrf2 antibody. Analysis of cell lysates cotransfected with Nrf2 and wild-type Keap1 (lane 3) as well as cell lysates cotransfected with Nrf2 and Keap1 ΔNTR (lane 4), ΔBTB (lane 5), ΔIVR (lane 6), ΔCTR (lane 7), or ΔDGR (lane 8) mutants are shown. Lane 1 is loaded with cell extract expressing only Keap1, and lane 2 is loaded with Nrf2 only. (*C*) Three domains (DGR, CTR, and IVR) are crucial for the Keap1 activity. Expression plasmids of Nrf2 (90 ng) and various Keap1 deletion mutants (shown in the figure; 10 ng) were transfected into NIH 3T3 cells ($2 \times 10^4$) along with a reporter plasmid, pNQO1-ARE (50 ng). Assays were performed in triplicate.

**DGR and CTR Are both Indispensable to Suppress the Transactivation Activity of Nrf2.** We then examined the ability of various Keap1 mutants to repress the transactivation activity of Nrf2 (Fig. 5*C*). Plasmids expressing Keap1 deletion mutants were cotransfected with plasmids expressing Nrf2 into NIH 3T3 cells along with the reporter plasmid (pNQO1-ARE) containing a single Nrf2-binding site. The luciferase activity attained by transfection of Nrf2 alone was set to 100% and used to normalize the relative activity in the presence of Keap1 mutants. Immunoblot analysis verified similar expression levels of each mutant protein (data not shown). Whereas Nrf2 activated the reporter gene expression >10-fold over the basal expression, simultaneous expression of Keap1 almost completely abolished this activation (compare lanes 1–3 in Fig. 5*C*). Transfection with ΔNTR and ΔBTB also markedly repressed the Nrf2 activity (Fig. 5*C*, lanes 4 and 5).

In contrast, deletion of the DGR and CTR from Keap1 almost abolished Keap1 activity in repressing transactivation of Nrf2 (Fig. 5*C*, lanes 7 and 8). Because ΔDGR and ΔCTR could not entrap Neh2-GFP in the cytoplasm (Fig. 4, ΔDGR and ΔCTR), these data suggest that both DGR and CTR are indispensable for Keap1 activity. Interestingly, deletion of IVR also affects the repressor activity of Keap1 (Fig. 5*C*, lane 6). This was an unexpected observation, because IVR does not interact directly with Nrf2 or actin (Figs. 2*B* and 5*A*). Four cysteine residues in IVR were recently shown to be highly reactive with electrophiles (16), and it was proposed that some of them act as sensors for electrophilic stimuli that regulate the association of Keap1 and Nrf2. The present result further supports our hypothesis that the cysteine residues in IVR are essential for Keap1 to repress the transactivation activity of Nrf2 (16).

## Discussion

We investigated in this study how a cytoplasmic protein Keap1 regulates Nrf2 activity. We found that Keap1 binds to the actin cytoskeleton and traps Nrf2, thereby preventing the nuclear translocation of this transcription factor. Whereas several Kelch-related proteins are known to colocalize with actin filaments, the physiological significance of the actin binding has not been well characterized (11). This study therefore provides the first convincing evidence that the direct interaction between Keap1 and the actin cytoskeleton contributes to the regulatory activity of Keap1. The present analyses further indicated that the DGR domain of Keap1 interacts primarily and directly with Nrf2, and the CTR and IVR domains also contribute to the ability of Keap1 to retain Nrf2 in the cytoplasm. Structure–function analyses of the Keap1–Nrf2 system provide plausible molecular understanding of how Keap1 functions as a sensor for inducing this signal pathway.

Keap1 colocalizes with the actin cytoskeleton and is abundantly distributed in the perinuclear region of the cytoplasm. This localization profile of Keap1 suggests three biological roles for Keap1. First, the perinuclear localization may allow Keap1 to entrap effectively Nrf2 protein synthesized *de novo* as it migrates into the nucleus. Second, because phase 1 enzymes that initially metabolize xenobiotics are usually localized on the cytoplasmic surface of the endoplasmic reticulum (23), Keap1 has easy access to the highly reactive phase 1 products by selecting actin filaments as a scaffold. Third, recently we and other groups found that Nrf2 is degraded rapidly and efficiently with the 26S proteasome under unstressed conditions (24–27). Because the proteasome is also known to colocalize with the actin filaments and intermediate filaments (28), we envisage that Keap1 may transfer the newly synthesized Nrf2 to the proteasome localized nearby, resulting in the rapid turnover of Nrf2.

CTR consists of 26 amino acid residues, and the primary structure is not well conserved among the other Kelch-related $\beta$-propeller proteins. CTR has one reactive cysteine (Cys-613), which binds dexamethasone mesylate (16). These results suggest a unique function of Keap1 CTR among Kelch family proteins. In the structure–function analysis of Keap1, CTR was shown to be essential for Keap1 repression of Nrf2. However, deletion of

CTR did not affect Keap1 interaction with Nrf2 in the immunoprecipitation analysis (Fig. 5*A*). One plausible explanation for this discrepancy is that CTR may act indirectly to modulate DGR activity. In contrast to the present results, it was recently reported that the presence of either DGR or CTR is sufficient for Keap1 to retain Nrf2 (29). In our experiments, however, the ΔDGR mutant possessing CTR could not repress Nrf2 activity at all, indicating that DGR is absolutely required for the Keap1 retention of Nrf2 in the cytoplasm. Zhang and Hannink (30) recently reported that 15 amino acid residues from C terminus of Keap1 are not required for the Keap1 activity, whereas in our experiments, ΔCTR (26-aa deletion) could not repress Nrf2 activity, indicating that CTR is required for the Keap1 activity.

Zipper and Mulcahy recently reported that Keap1 forms a homodimeric complex through the BTB domain (9). Keap1 dimerization was suggested to be an important step for sequestration of Nrf2 in the cytoplasm and the Ser-104 residue in the BTB domain appeared to be critical for Keap1 self-association. In contrast, we found that ΔBTB-Keap1 effectively repressed Nrf2 transactivation activity (Fig. 5*C*, lane 5). Thus, deletion of the BTB domain did not impair Keap1 activity in our transfection analysis. We surmise that this discrepancy may be due to differences in the experimental conditions. Whereas the BTB domain is not the direct binding interface, it is possible that this domain may modulate the function of the DGR domain, as is the case for CTR and IVR domains.

Transcriptional regulation through the actin cytoskeleton seems to be unique to the Keap1–Nrf2 system. In this regard, it is noteworthy that Cubitus interruptus (Ci) of *Drosophila*, which is a transcription factor under the Hedgehog signal pathway (31), may have some similarity to the Keap1–Nrf2 system. In the absence of ligand Hedgehog, Ci is tethered to microtubules through forming a complex with Fused, Cos2, and Su(fu) proteins. On Hedgehog binding to the receptor Patched, an inhibitor protein Smoothened is released and it liberates Ci from microtubules. The microtubule association seems to be essential for Ci, because Slimb associated with microtubules modifies Ci to a transcriptional repressor through cleavage. Because Keap1-mediated tethering of Nrf2 to the actin cytoskeleton provokes degradation of Nrf2 (26, 27), the actin cytoskeleton seems to provide a scaffold for protein modification and degradation in the Keap1–Nrf2 system.

We thank Drs. Paul Talalay, Pamela Talalay, Makoto Kobayashi, Albena Dinkova-Kostova, Hozumi Motohashi, Ken Itoh, and Thomas W. Kensler for help and discussion. This work was supported in part by grants from Japan Science and Technology Agency–Exploratory Research for Advanced Technology (to M.Y.), the Ministry of Education, Sciences, Sports, and Technology (to A.K. and M.Y.), and the Ministry of Health, Labor, and Welfare (to M.Y.).

1. Nguyen, T., Sherratt, P. J. & Pickett, C. B. (2003) *Annu. Rev. Pharmacol. Toxicol.* **43**, 233–260.
2. Moi, P., Chan, K., Asunis, I., Cao, A. & Kan, Y. W. (1994) *Proc. Natl. Acad. Sci. USA* **91**, 9926–9930.
3. Itoh, K., Igarashi, K., Hayashi, N., Nishizawa, M. & Yamamoto, M. (1995) *Mol. Cell. Biol.* **15**, 4184–4193.
4. Itoh, K., Chiba, T., Takahashi, S., Ishii, T., Igarashi, K., Katoh, Y., Oyake, T., Hayashi, N., Satoh, K., Hatayama, I., *et al.* (1997) *Biochem. Biophys. Res. Commun.* **236**, 313–322.
5. Ishii, T., Itoh, K., Takahashi, S., Sato, H., Yanagawa, T., Katoh, Y., Bannai, S. & Yamamoto, M. (2000) *J. Biol. Chem.* **275**, 16023–16029.
6. Motohashi, H., O'Connor, T., Katsuoka, F., Engel, J. D. & Yamamoto, M. (2002) *Gene* **294**, 1–12.
7. Itoh, K., Wakabayashi, N., Katoh, Y., Ishii, T., Igarashi, K., Engel, J. D. & Yamamoto, M. (1999) *Genes Dev.* **13**, 76–86.
8. Xue, F. & Cooley, L. (1993) *Cell* **72**, 681–693.
9. Zipper, L. M. & Mulcahy, R. T. (2002) *J. Biol. Chem.* **277**, 36544–36552.
10. Ito, N., Phillips, S. E., Yadav, K. D. & Knowles, P. F. (1994) *J. Mol. Biol.* **238**, 794–814.
11. Adams, J., Kelso, R. & Cooley, L. (2000) *Trends Cell Biol.* **10**, 17–24.
12. Kim, L F., Mohammadi, E. & Huang, R. C. (1999) *Gene* **228**, 73–83.
13. Hayes, J. D., Chanas, S. A., Henderson, C. J., McMahon, M., Sun, C., Moffat, G. J., Wolf, C. R. & Yamamoto, M. (2000) *Biochem. Soc. Trans.* **28**, 33–41.
14. Wakabayashi, N., Itoh, K., Wakabayashi, J., Motohashi, H., Noda, S., Takahashi, S., Imakado, S., Kotsuji, T., Otsuka, F., Roop, D. R., *et al.* (2003) *Nat. Genet.* **35**, 238–245.
15. Dinkova-Kostova, A. T., Massiah, M. A., Bozak, R. E., Hicks, R. J. & Talalay, P. (2001) *Proc. Natl. Acad. Sci. USA* **98**, 3404–3409.
16. Dinkova-Kostova, A. T., Holtzclaw, W. D., Cole, R. N., Itoh, K., Wakabayashi, N., Katoh, Y., Yamamoto, M. & Talalay, P. (2002) *Proc. Natl. Acad. Sci. USA* **99**, 11908–11913.
17. Niwa, H., Yamamura, K. & Miyazaki, J. (1991) *Gene* **108**, 193–200.
18. Bubb, M. R., Spector, I., Bershadsky, A. D. & Korn, E. D. (1995) *J. Biol. Chem.* **270**, 3463–3466.
19. Jordan, A., Hadfield, J., Lawrence, N. J. & McGown, A. T. (1998) *Med. Res. Rev.* **18**, 259–296.
20. Theodoropoulos, P. A., Gravanis, A., Tsapara, A., Margioris, A. N., Papadogiorgaki, E., Galanopoulos, V. & Stournaras, C. (1994) *Biochem. Pharmacol.* **47**, 1875–1881.
21. Kang, K. W., Lee, S. J., Park, J. W. & Kim, S. G. (2002) *Mol. Pharmacol.* **62**, 1001–1010.
22. Soltysik-Espanola, M., Rogers, R. A., Jiang, S., Kim, T. A., Gaedigk, R., White, R. A., Avraham, H. & Avraham, S. (1999) *Mol. Biol. Cell* **10**, 2361–2375.
23. Guengerich, F. P. (1990) *Crit. Rev. Biochem. Mol. Biol.* **25**, 97–153.
24. Nguyen, T., Sherratt, P. J., Huang, H. C., Yang, C. S. & Pickett, C. B. (2003) *J. Biol. Chem.* **278**, 4536–4541.
25. Stewart, D., Killeen, E., Naquin, R., Alam, S. & Alam, J. (2002) *J. Biol. Chem.* **18**, 2396–2402.
26. McMahon, M., Itoh, K., Yamamoto, M. & Hayes, J. D. (2003) *J. Biol. Chem.* **278**, 21592–21600.
27. Itoh, K., Wakabayashi, N., Katoh, Y., Ishii, T., O'Connor, T. & Yamamoto, M. (2003) *Genes Cells* **8**, 379–391.
28. Arcangeletti, C., Sutterlin, R., Aebi, U., De Conto, F., Missorini, S., Chezzi, C. & Scherrer, K. (1997) *J. Struct. Biol.* **119**, 35–58.
29. Dhakshinamoorthy, S. & Jaiswal, A. K. (2001) *Oncogene* **20**, 3906–3917.
30. Zhang, D. D. & Hannik, M. (2003) *Mol. Cell. Biol.* **23**, 8137–8151.
31. Aza-Blanc, P. & Kornberg, T. B. (1999) *Trends Genet.* **5**, 458–462.

# Small Maf proteins serve as transcriptional cofactors for keratinocyte differentiation in the Keap1–Nrf2 regulatory pathway

Hozumi Motohashi*, Fumiki Katsuoka*, James Douglas Engel†, and Masayuki Yamamoto*‡§

*Institute of Basic Medical Sciences and Center for Tsukuba Advanced Research Alliance and ‡Exploratory Research for Advanced Technology, Environmental Response Project, University of Tsukuba, Tsukuba 305-8577, Japan; and †Department of Cell and Developmental Biology and Center for Organogenesis, University of Michigan, Ann Arbor, MI 48109-0616

Edited by Mark T. Groudine, Fred Hutchinson Cancer Research Center, Seattle, WA, and approved March 9, 2004 (received for review September 12, 2003)

**The small Maf proteins, MafF, MafG, and MafK, possess a leucine zipper (Zip) domain that is required for homodimer or heterodimer complex formation with other bZip transcription factors. In this study we sought to determine the identity of the specific constituent that collaboratively interacts with Nrf2 to bind to the Maf recognition element *in vivo*. Studies *in vitro* suggested that Nrf2 forms heterodimers with small Maf proteins and then bind to Maf recognition elements, but the bona fide partner molecules supporting Nrf2 activity *in vivo* have not been definitively identified. Nrf2 activity is usually suppressed by a cytoplasmic repressor, Keap1, so disruption of the *keap1* gene causes constitutive activation of Nrf2. Nrf2 hyperactivity results in hyperproliferation of keratinocytes in the esophagus and forestomach leading to perinatal lethality. However, simultaneous disruption of *nrf2* rescued *keap1*-null mice from the lethality. We exploited this system to investigate whether small Mafs are required for Nrf2 function. We generated *keap1* and small *maf* compound mutant mice and examined whether keratinocyte abnormalities persisted in these animals. The data show that loss of *mafG* and *mafF* in the *keap1*-null mice reversed the lethal keratinocyte dysfunction and rescued the *keap1*-null mutant mice from perinatal lethality. This rescue phenotype of *mafG::mafF::keap1* triple compound mutant mice phenocopies that of the *nrf2::keap1* compound mutant mice, indicating that the small Maf proteins MafG and MafF must functionally cooperate with Nrf2 *in vivo*.**

A central issue in deciphering the regulatory mechanisms mediated by the activity of transcription factors is how to best evaluate the *in vivo* contribution of each protein–protein and transcription factor–DNA interaction that is defined *in vitro*. Transcription factors that interact with Maf recognition elements (MARE) possess a basic region-leucine zipper (bZip) domain and form dimers that can be characterized by a potentially enormous combinatorial array (1). *In vitro* analysis has shown that MARE binding complexes consist mainly of: (*i*) four large Maf or three small Maf protein homodimers; (*ii*) heterodimer complexes containing a small Maf with any of six different Cap-N-Collar (CNC) family proteins; and (*iii*) homo- or heterodimers composed of Jun and Fos family members (2–4). To elucidate MARE-dependent gene regulatory mechanisms, we need to identify the major participants among all these possible interacting molecules in an *in vivo* context.

The small Maf proteins, MARE-binding components that were originally identified as cellular homologs of the v-*maf* oncogene (4–6), dimerize among themselves and with other bZip factors, usually CNC or Bach family proteins (7–11). The small Maf family consists of only three members, MafF, MafG, and MafK, but to date, other than their differential tissue distribution (12), no functional differences among the three have been revealed. The CNC family includes NF-E2 p45, Nrf1, Nrf2, and Nrf3 (7, 9, 13, 14), and Bach family proteins are closely related to CNC members (10). While small Maf proteins lack any recognizable transcriptional effector domains, CNC and Bach families possess transactivation or -repression domains unique to each molecule. Through heterodimerization, the small Maf protein confers DNA-binding specificity to its CNC or Bach partner molecule on the MARE sequence, and enables these heterodimers to execute differential activating or repressing activities as dictated by their encoded functional domains.

The Maf proteins recognize either a T-MARE, containing a TPA responsive element (TRE), or a C-MARE, containing a cAMP responsive element (CRE) as a core sequence. In these MAREs, the core consensus motifs are flanked on each side by three conserved residues "TGC" and "GCA" at the 5′ and 3′ ends, respectively. The DNA binding specificity of Maf proteins is achieved through their inherent recognition of these flanking sequences, whereas the other bZip factors, such as Nrf2 and Fos, recognize primarily the TRE or CRE core sequences. A previous NMR study revealed that the structural basis for the unique "GC" requirement of Maf proteins for DNA binding is caused by the presence of an extended homology region, which is conserved only within the Maf family (15).

Germ-line mutagenesis of the *nrf2* gene revealed that Nrf2 is an essential component for antioxidant and detoxification enzyme gene expression (16). Nrf2 transcriptional activity is controlled by an interaction between Nrf2 and the cytoplasmic regulatory protein Keap1 (17). When cells are exposed to electrophiles or reactive oxygen species (ROS), Nrf2 is released from Keap1 cytoplasmic capture, leading to its translocation to the nucleus, where Nrf2 activates transcription of target genes. The marked susceptibility of *nrf2*-null mutant mice to the toxicity of electrophiles and ROS demonstrates the importance of Nrf2 for protection against oxidative stress (18–20). We therefore generated *keap1*-null mutant mice, anticipating that Nrf2 might be constitutively activated in the absence of Keap1, thereby conferring resistance to electrophilic stress. To our surprise, the *keap1*-null mutant mice died before weaning due to a hyperkeratotic proliferative disorder (21). The cornified layers of esophageal and forestomach stratified squamous epithelia were abnormally thickened, thereby obstructing the lumen. We found that this epithelial phenotype was completely rescued by the additional disruption of *nrf2*, indicating that the *keap1*-null phenotype reflects a gain of Nrf2 function.

There has been some uncertainty regarding the identity of the heterodimeric partner molecule of Nrf2 *in vivo*. *In vitro* studies have shown strong DNA binding activity of Nrf2-small Maf heterodimers (16, 22, 23), which supported our contention that this complex actually functions as a major transcriptional activator *in vivo*. However, although strong transactivation activity was observed when Nrf2 was overexpressed in culture cells, addition of small Maf to the transfection reaction led to reporter

This paper was submitted directly (Track II) to the PNAS office.

Abbreviations: MARE, Maf recognition element; CNC, Cap-N-Collar.

§To whom correspondence should be addressed. E-mail: masi@tara.tsukuba.ac.jp.

gene repression in most cases (22, 24–26). Hence, the question we sought to answer was whether or not the Nrf2/small Maf heterodimer is the functionally active species that acts at MAREs *in vivo*.

Alternative candidates for heterodimeric partner molecule of Nrf2 have been suggested. For example, c-Jun and ATF-4 were reported to cooperate with Nrf2 for gene activation *in transfecto* (27, 28). However, because disruption of *c-jun* or *atf-4* does not cause a defect similar to that observed in *nrf2*-null mutant animals (29–31), it remains to be clarified whether these factors can heterodimerize with Nrf2 to transduce transcriptional responses from MAREs *in vivo*. Similarly, a functional contribution of small Maf proteins to Nrf2 activity has not been well documented in small *maf* mutant mice.

Because disruption of the *keap1* gene causes severe dysfunction of keratinocytes that leads to perinatal lethality, but simultaneous disruption of *nrf2* rescued *keap1*-null mice from the lethality, we exploited this compound knockout–rescue approach to investigate whether small Mafs actually function cooperatively with Nrf2 and activate transcription *in vivo*. To this end, we generated *keap1*::small *maf* compound knockout mutant mice and examined whether a reduction in small Maf activity, as does the loss of Nrf2, mitigates the *keap1*-null phenotype. We show here that simultaneous disruption of the *mafG* and *mafF* genes rescued the *keap1*-null pups from perinatal lethality, allowing them to survive to adulthood. Thus, the small *maf*::*keap1* mutant mice phenocopy the rescue phenotype of *nrf2*::*keap1* compound mutant mice, demonstrating that the small Maf proteins cooperatively function with Nrf2 *in vivo*.

## Materials and Methods

**Generation of the Small *maf*::*keap1* Compound Mutant Mice.** Germline mutagenesis of the murine *mafF*, *mafG*, *mafK*, *nrf2*, and *keap1* genes has been described (12, 16, 21, 32). All of the mice examined in this study were of mixed genetic background with contributions from 129Sv/J, C57BL/6J, and ICR. Genotypes were determined by PCR. The body weight of each mouse was measured weekly. More than three independent animals of each genotype were first weighed on postnatal day 7, and then followed to the 6th week.

**Histological Analysis.** Two-day-old pups, 10- to 12-day-old pups, and 4-month-old mice were killed, and the forestomach was dissected. Samples for staining with hematoxylin and eosin were fixed in 3.7% formaldehyde overnight and then embedded in paraffin. LacZ staining was performed as described (33). Samples for immunostaining with antibodies against Nrf2 or keratin 6 were fixed in PBS containing 1% formaldehyde, 0.2% glutaraldehyde, and 0.02% Nonidet P-40 for 30 min, embedded in OCT compound (Tissue-tek, Sakura Finetechnical, Chuo-ku, Tokyo), followed by frozen sectioning with a cryostat. The antibody against Nrf2 (C-20, Santa Cruz Biotechnology) was used at a 1:400 dilution; immunoreactivity was visualized with an avidin-biotin-peroxidase kit (Vector Laboratories). The antibody recognizing keratin 6 (PRB-169P, Covance, Princeton) was used at a 1:500 dilution.

**Quantitative Real-Time PCR.** Total RNA was extracted from the forestomach of 10- to 12-day-old pups using ISOGEN (Nippon Gene, Toyama, Japan). Random cDNA was synthesized from the isolated RNAs, and real-time PCR (ABI PRISM 7700) was performed as described (12) with minor modifications. To measure the copy number of each mRNA, plasmids harboring each cDNA were used as standards. Oligonucleotide sequences used for detecting MafF mRNA are available upon request.

**RNA Blot Analysis.** Total RNA was prepared as described above. Total RNA (2 $\mu$g per lane) was used for electrophoresis, followed by hybridization to radiolabeled probes. The keratin 6 probe was generated by PCR (primer sequences are available upon request). The PCR product was cloned, sequenced, and used as a probe for detecting the transcripts of both keratin 6 genes (i.e., keratin 6a and keratin 6b).

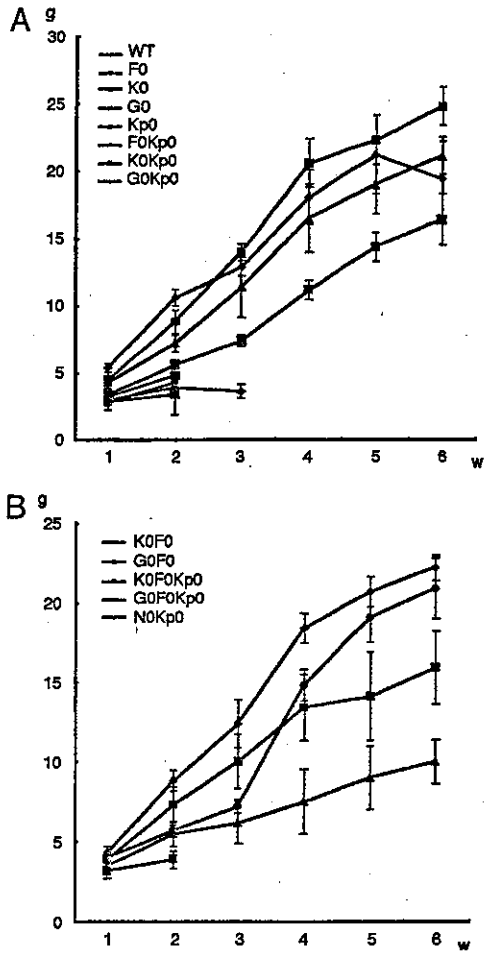


**Fig. 1.** Small *maf*::*keap1* compound mutant mice survive beyond weaning. (*A*) Body weight change for mice bearing single small *maf* gene disruptions in the *keap1*-null background. Deletion of either *mafK* or *mafF* did not extend the lifespan of *keap1*-null mutant pups. When *mafG* alone was disrupted in addition to *keap1*, pups survived one week longer. (*B*) Body weight change for mice with compound small *maf* gene disruptions in the *keap1*-null mutant background. Simultaneous deletion of *mafG* and *mafF* rescued the lethality of *keap1*-null mutant pups. The body weight of *nrf2*::*keap1* mice was examined as a control. WT indicates wild-type; F0, *mafF*−/−; K0, *mafK*−/−; G0, *mafG*−/−; N0, nrf2−/−; Kp0, *keap1*−/−.

## Results

**Simultaneous Loss of *mafG* and *mafF* Rescues *keap1*-Null Mutant Postnatal Lethality.** To ask whether a reduction in small Maf activity mitigates the *keap1*-null phenotype, we crossed small *maf* mutant mice with *keap1* mutants to generate compound mutant animals. When *mafK* or *mafF* was deleted in addition to *keap1*, no pups survived beyond weaning (Fig. 1*A*; precisely the same phenotype as in the *keap1* mutants), but the life span of *mafG*::*keap1* compound mutant mice was approximately one week longer than mice bearing only the *keap1* mutant alleles (Fig. 1*A*, G0Kp0 mice), suggesting that the *mafG* contribution to keratinocytic homeostasis is greater than that of either MafK or MafF.

Because the results of small *maf* compound mutant analyses indicate that three small Mafs are capable of compensating for one another (34), we next further reduced the number of active small *maf* alleles in the *keap1*-null background. Whereas mice bearing disruptions in all three small *maf* genes might have been preferred

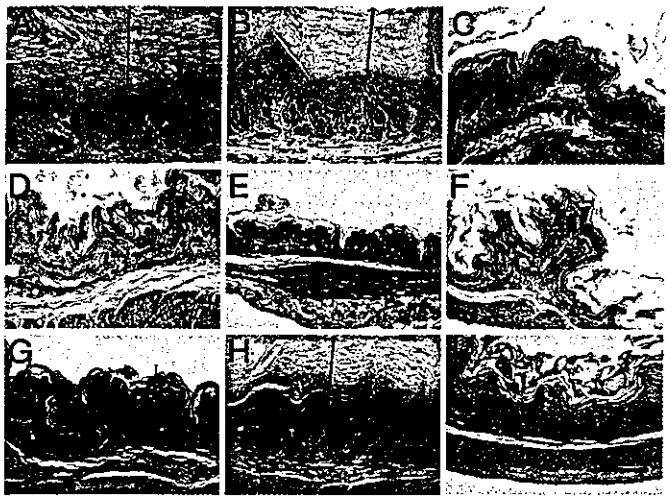

Fig. 2. Histological examination of forestomach. Hematoxylin/eosin staining of 10-day-old forestomach thin sections from Kp0 (*A*), F0Kp0 (*B*), G0F0Kp0 (*C*), WT (*D*), F0 (*E*), and G0F0 (*F*) pups are shown. Sections of the forestomach from 4-month-old mice of WT (*G*), G0F0Kp0 (*H*), and N0Kp0 (*I*) genotypes are also presented. Double-ended arrows indicate the cornified layer. (Scale bar, 150 μm.)

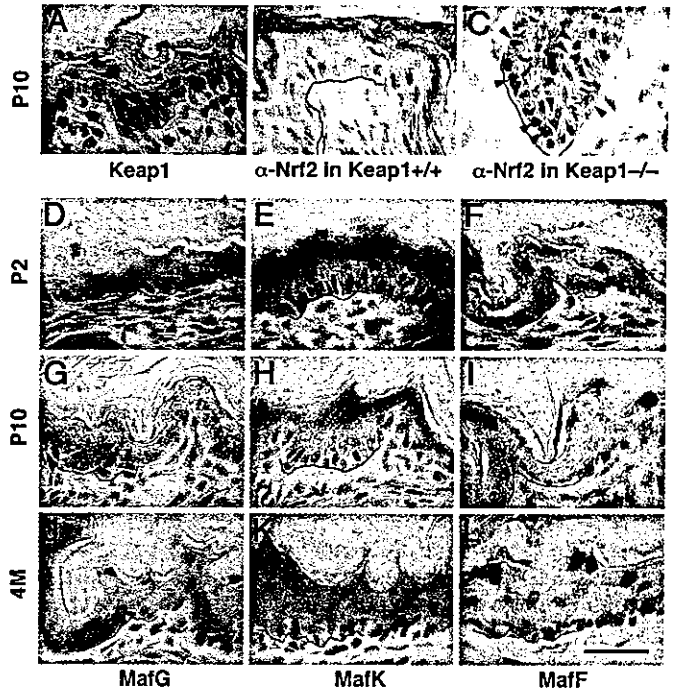


Fig. 3. Expression profiles of Keap1, Nrf2, and small Mafs in the forestomach. (*A*) LacZ staining of squamous cell epithelia in the forestomach of *keap1* heterozygous mutant mice. Blue staining is observed in LacZ-expressing cells. (*B* and *C*) Immunohistochemistry with anti-Nrf2 antibody. Brown punctate staining, indicated by arrowheads, is observed within nuclei of *keap1*-null mutant cells (*C*), whereas no staining develops in wild-type keratinocytes (*B*). Nonspecific staining is observed in the cornified epithelial layers. (*D–L*) LacZ staining of squamous cell epithelia of the forestomach in sections prepared from *mafG* (*D*, *G*, and *J*), *mafK* (*E*, *H*, and *K*), and *mafF* (*F*, *I*, and *L*) heterozygous mutant mice. Samples were prepared from 2-day-old (*D–F*), 10-day-old (*G–I*), or 4-month-old (*J–L*) mice. The green lines indicate the position of basement membranes. (Scale bar, 30 μm throughout.)

for this analysis, mice lacking all small Mafs die by midgestation (unpublished observations). Similarly, *mafG::mafK* compound mutant mice expire before weaning (34). We therefore examined instead two genotypes that were healthy and fertile (i.e., *mafG::mafF* and *mafF::mafK* compound mutants) in combination with the mutant *keap1*-null alleles (Fig. 1*B*). Whereas disruption of both *mafK* and *mafF* did not rescue *keap1* mutant from lethality (K0F0Kp0 mice), when the *mafG* and *mafF* genes were simultaneously deleted in the *keap1*-null background the mice survived for more than four months (G0F0Kp0 mice in Fig. 1*B*).

Because we previously found that the simultaneous deletion of *nrf2* with *keap1* genes almost completely reversed the *keap1*-null mutant phenotype (21), we compared the body weight gain of G0F0Kp0 mice with that of *nrf2::keap1* compound mutant mice (N0Kp0 mice) to evaluate the efficiency of the rescue by simultaneous *mafG* and *mafF* deletion. Whereas N0Kp0 mice showed a similar body weight gain to that of wild-type mice, G0F0Kp0 mice were much smaller than both of these at 6 weeks after birth (Fig. 1). G0F0Kp0 mice were also smaller than G0F0 mice (G0F0Kp0 vs. G0F0 in Fig. 1*B*), indicating that the effect of the Keap1 deficiency is only partially overcome in G0F0Kp0 mice. These results demonstrate that Keap1 deficiency provokes constitutive activation of Nrf2 and the growth retardation of mice, but this deleterious effect of Keap1 loss can be partially circumvented by the simultaneous loss of MafG and MafF.

**Improvement of Hyperkeratosis in Forestomach and Esophagus of *mafG::mafF::keap1* Triple Mutant Mice.** We next performed histological analysis of the forestomach and esophagus of the rescued triple compound mutant (i.e., G0F0Kp0) animals at 10 days after birth (Fig. 2 and data not shown). Heavily thickened cornified layers, convoluted basal layers, and thickened spinous and granular layers were observed in the forestomach of *keap1*-null mutant and F0Kp0 mice (Fig. 2 *A* and *B*), whereas G0F0Kp0 mice displayed a normal stratified squamous epithelium (Fig. 2*C*), similar to the control samples (Fig. 2 *D–F*).

Because the body weight difference was apparent between G0F0Kp0 and N0Kp0 mice at 6 weeks of age, we hypothesized that the constitutive elevation of Nrf2 activity in the *keap1*-null background was only partially overcome in G0F0Kp0 mice and that the rescue of the *keap1*-null phenotype might be incomplete. In support of this contention, we found that the forestomach epidermal layers of G0F0Kp0 mice were hyperkeratotic, whereas those of the N0Kp0 forestomach were almost indistinguishable from wild type (Fig. 2 *G–I*). We envisage that in contrast to *keap1*-null mutant mice, thickening of the cornified epithelial layers develop more gradually in the G0F0Kp0 forestomach as a consequence of residual elevated Nrf2 activity.

**Keratinocyte Abnormality Is Involved in the Hyperkeratosis Observed in *keap1*-Null Mice.** To determine whether diminished Keap1 expression in keratinocytes might lead to the observed hyperkeratosis, we examined *keap1* gene expression in the stratified squamous epithelium by monitoring the expression of the *LacZ* gene that was inserted into the *keap1* locus when the gene was disrupted (21). β-Galactosidase activity was observed primarily in keratinocytes of whole layers of stratified squamous epithelium, from the immature cells in basal layers to the granular layers composed of more differentiated cells (Fig. 3*A*). The green lines in Fig. 3 define the position of the basement membrane. These data indicate that Keap1 is predominantly expressed in keratinocytes, regardless of differentiation stage.

We next examined Nrf2 activation in the unstimulated, but pathologically expanded, forestomach epithelium of *keap1*-null mutant mice by examining the epithelial cells for nuclear accumulation of Nrf2 protein. Keap1 sequesters Nrf2 in the cytoplasm and prevents it from traversing into the nucleus (17). Recent reports showed that Nrf2 is constantly degraded by the proteasome when cells are not stimulated (35–38), thus keeping Nrf2 concentration

BIOCHEMISTRY

low, whereas Nrf2 is translocated into the nucleus and is stabilized upon exposure to electrophilic reagents or oxidative stress. We performed immunohistochemical examination of the keratinocytes of *keap1*-null animals using an antibody that specifically recognizes Nrf2. As expected, intranuclear foci were observed in the forestomach epithelium of the *keap1*-null mutant mice (Fig. 3*C*, arrowheads); also as anticipated, no Nrf2 was detected in comparable cells of a wild-type littermate (Fig. 3*B*), consistent with the notion that proteasome-mediated turnover leads to rapid degradation of Nrf2 in the unstimulated cytoplasm. These results thus demonstrate that the control processes mediated by Nrf2 and Keap1 are actually extant in forestomach keratinocytes. The results also suggest that gene dysregulation within keratinocytes is involved in the hyperkeratosis observed in *keap1*-null mutant mice.

**Small Maf Proteins Are Expressed in Forestomach Keratinocytes.** The rescue experiments described above suggest that diminished small Maf activity is required for correction of the *keap1*-induced keratinocytic abnormality, and that the small Mafs must therefore act in the same genetic pathway as Nrf2 to execute the transcriptional program in keratinocyte differentiation (Fig. 1). However, none of the small *maf* mutant phenotypes described to date include keratinocytic abnormalities; no report has emerged demonstrating any functional contribution of small Mafs to keratinocyte biology.

Therefore, we examined the expression of the three small *maf* genes in the forestomach epithelium by monitoring LacZ activity in the small *maf* mutants, because each of the small *maf* knockouts was generated by simultaneous insertion of a *LacZ* gene. While we inserted the normal *LacZ* gene into the *mafK* and *mafG* loci, the *mafF* insertion contained lacZ linked to a nuclear localization signal (NLS). At 10 days after birth, β-galactosidase activity was observed throughout the layers of stratified squamous epithelium in the *mafG* mutant mice (Fig. 3*G*). Expression of *mafK* is weaker in the basal cells and stronger in more differentiated cells of the spinous and granular layers (Fig. 3*H*). Interestingly, *mafF* is expressed almost exclusively in the most differentiated granular layer cells (Fig. 3*I*). β-Galactosidase activity was localized in the cytoplasm of keratinocytes in *mafK* and *mafG* mutant mice, which gave rise to both diffuse and punctate staining (Fig. 3 *G* for *mafG* and *H* for *mafK*), but the activity was exclusively nuclear in keratinocytes of *mafF* mutant mice (Fig. 3*I*). These expression patterns were reproducible when 2-day-old pups and 4-month-old adult mice were analyzed for each small *maf* gene (Fig. 3 *D–F* and *J–L*). β-Galactosidase staining was especially intense in the granular layer of *mafK* mutant mice, regardless of developmental stage (Fig. 3 *E*, *H*, and *K*). The abundance of all three small *maf* gene mRNAs was almost constant from neonatal stages to adulthood, when monitored by quantitative real-time PCR (data not shown). Thus, all three small Maf proteins are expressed in the forestomach squamous epithelium, and the expression patterns are indeed overlapping with those of Nrf2 and Keap1.

**MafG Is a Major Small Maf Protein Species in Keratinocytes.** To determine whether there were any correlations between the mRNA abundance and the functional contribution of each small *maf* gene, the copy numbers of each small Maf mRNA expressed in the forestomach at 10 days after birth were quantified by quantitative real-time PCR, and MafG mRNA was found to be the most abundant small Maf (Fig. 4). The observed abundant MafG expression in the forestomach shows very good agreement with the data in the small *maf* gene knockout–rescue experiments (Fig. 1), which suggest that MafG makes the largest contribution to normal keratinocyte function among the three small Maf proteins. We conclude that *mafG* and *mafF* disruption attained a significant enough reduction in the total amount of small Maf protein that there was no longer sufficient Maf activity present in cells to effectively execute Nrf2 function.

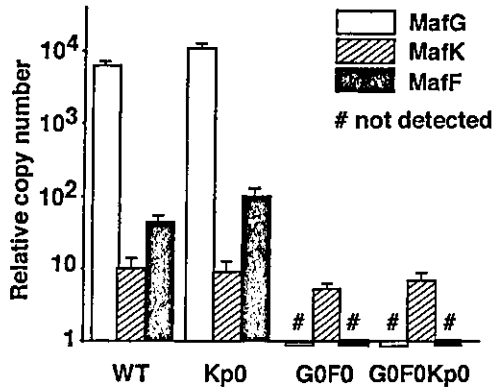


Fig. 4. Quantification of small Maf mRNA abundance in forestomach. cDNA was synthesized from total RNA prepared from WT, Kp0, G0F0, and G0F0Kp0 forestomach at 10 days after birth. MafG, MafK, and MafF mRNA levels were quantified by quantitative real-time PCR using a plasmid containing each cDNA as the abundance standard.

**Increased Keratin 6 Expression Returns to Normal Levels in the Forestomach of *mafG::mafF::keap1* Triple Mutant (Rescued) Mice.** Keratin 6 is strongly induced in the *keap1*-null mutant esophagus, and it has been suggested to be a direct Nrf2 target gene in keratinocytes. The expression of keratin 6 was dramatically induced in the forestomach epithelium of the *keap1*-null mice, judging from the strong immunohistochemical anti-keratin 6 staining (Fig. 5 *A* and *B*). Consistent with the distribution of constitutively activated Nrf2 in the *keap1* mutant mice (see Fig. 3*C*), keratin 6 was induced in all keratinocyte layers (Fig. 5*B*). To investigate whether increased keratin 6 expression in the *keap1*-null mutant forestomach is caused by constitutive activation of Nrf2, we analyzed keratin 6 expression in N0Kp0 compound mutant mice. Keratin 6 mRNA was abundant in the *keap1* mutant (Fig. 5*D*, lanes 3 and 4), but was scarcely detectable in either the wild-type or N0Kp0 animals (Fig. 5*D*, lanes 1, 2, 11, and 12), thus confirming the Nrf2-dependency of *keratin 6* gene activation.

We then examined the expression of keratin 6 in the rescued G0F0Kp0 mice. Application of anti–keratin 6 antibody did not generate a signal in the forestomach epithelial layers of G0F0Kp0 mice (Fig. 5*C*), and, as in the N0Kp0 mutant, the G0F0Kp0 mutant forestomach expressed the same low levels of keratin 6 mRNA as wild-type mice (Fig. 5*D*, lanes 9 and 10). These results thus demonstrate that the small Maf proteins are required for Nrf2-dependent transcriptional activation of the *keratin 6* gene.

Although the double deletion of *mafF* and *mafG* rescued the lethality of *keap1* null mutants, *mafF* deletion alone did not affect the lifespan of *keap1*-null pups (F0Kp0 in Fig. 1), and ablation of *mafG* extended their lifespan by only one week (G0Kp0 in Fig. 1). These results suggested that the rescue efficiency of each compound mutant mouse inversely correlates with the remaining small Maf activity; Kp0 mice possess full activity, and small Maf abundance in keratinocytes appears to be reduced in the order: F0Kp0 > G0Kp0 > G0F0Kp0. Hence we hypothesized that the expression of keratin 6 mRNA would be higher in the order: Kp0 > F0Kp0 > G0Kp0 > G0F0Kp0. In the hope of detecting graded expression of keratin 6 mRNA, we further examined G0Kp0 and F0Kp0 mice.

Contrary to our expectation, keratin 6 mRNA was hardly detectable except in the Kp0 and F0Kp0 mutants (Fig. 5*D*, lanes 1, 2, and 7–12). Considering the similarity in low-level expression of keratin 6 in G0Kp0 and G0F0Kp0 mice, some additional factors may be involved in the large difference in weight gain and viability between the mice of two genotypes. A second unexpected result was that keratin 6 is more abundant in *mafF::keap1* double mutant than *keap1* single mutant forestomach (Fig. 5*D*, lanes 3–6). Interestingly, when small *maf* expression levels were examined, *mafG* was found

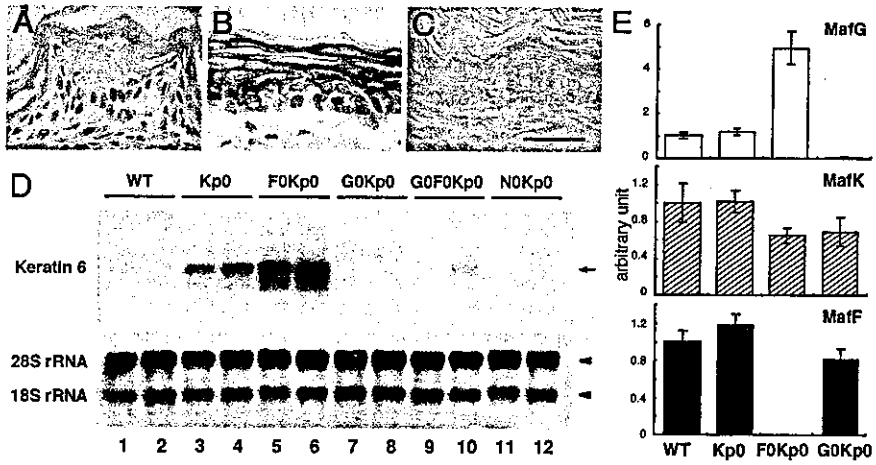


**Fig. 5.** Expression of keratin 6 as a marker of Nrf2-mediated transcriptional activity. (*A–C*) Immunohistochemistry with anti-keratin 6 antibody. Keratin 6 is highly expressed in *keap1*-null keratinocytes in the forestomach (*B*), whereas no signals were observed in the wild-type (*A*) or rescued G0F0Kp0 (*C*) mice. (Scale bar, 30 $\mu$m in *A–C*.) (*D*) Keratin 6 expression levels were examined by RNA blot analysis. Total RNA prepared from wild-type (lanes 1 and 2), Kp0 (lanes 3 and 4), F0Kp0 (lanes 5 and 6), G0Kp0 (lanes 7 and 8), G0F0Kp0 (lanes 9 and 10), and N0Kp0 (lanes 11 and 12) mice forestomachs are shown. The arrow and arrowheads indicate keratin 6 mRNA and ribosomal RNAs (18S and 28S), respectively. (*E*) Relative expression levels of the three small *maf* genes in the forestomach of wild-type, Kp0, F0Kp0, and G0Kp0 at 10 days after birth (compared with the levels in wild-type mice).

to be highly induced in *mafF::keap1* double mutant forestomach (Fig. 5*E*).

## Discussion

It has been postulated that the small Maf proteins function as major heterodimeric partner molecules of Nrf2 based principally on *in vitro* DNA binding evidence. Heterodimer formation between Nrf2 and the small Mafs was detected by using bacterially expressed proteins or *in vitro* translated proteins (14, 16, 22, 24, 28, 39, 40), and substantial efforts have been made to document endogenous Nrf2-small Maf complexes capable of interacting with MAREs (23, 25, 41, 42). Although these studies have shown Nrf2-small Maf heterodimer formation, the question remained whether Nrf2-small Maf heterodimer actually functions as a transcription activator or whether Nrf2 might require an alternative partner to activate MARE-dependent target genes, because in many transfection assays cooperative activation of Nrf2 and small Mafs was not observed (22, 24–26). Hence the aim of this study was to test the contention that small Mafs cooperate with Nrf2 to activate transcription in an *in vivo* experimental system.

To address this issue, we generated *keap1* and small *maf* compound gene knockout mice and asked whether the loss of one or two small *maf* genes in concert with the *keap1* gene affected the lethal phenotype of Keap1-null mutant mice caused by the hyperactivity of Nrf2. We found that loss of *mafG* and *mafF* indeed rescued the *keap1*-null mutant mice from perinatal lethality. Because the rescue phenotype of *mafG::mafF::keap1* triple compound mutant mice is similar to that of the *nrf2::keap1* compound mutant mice, we conclude that small Maf proteins are indispensable components for Nrf2-dependent transcription *in vivo*. These results further support the contention that Nrf2-small Maf heterodimers serve as indispensable transcriptional regulators of keratinocytic gene expression.

We suggested previously that *loricrin* and *keratin 6* are potential Nrf2 target genes in keratinocytes (21). There is one potential MARE in *loricrin* "CCA*TGGTGACATAGC*TTGAA", and two MAREs in *keratin 6*, "TGA*TGGTGAGC*TT*GCA*GAGT," and "GTG*TGGTGAGGGGGCA*CACA," ≈40 bp and 300 bp 5′ to the TATA boxes, respectively (nucleotides corresponding to a typical T-MARE, "TGCTGA$^{G}/_{C}$TCAGCA," are italicized). These sequences correspond closely to the consensus sequence of antioxidant responsive elements (ARE), well characterized Nrf2 target sites that exist in the regulatory regions of phase 2 detoxifying enzyme genes and oxidative stress-inducible genes (43). In this study, we monitored *keratin 6* as a parameter for measuring Nrf2 transcriptional activity, because the expression profile of *keratin 6* corresponds closely to the distribution of Keap1-Nrf2 system in forestomach (see Fig. 5 *A* and *B*). Importantly, the increase in expression of *keratin 6* observed in the *keap1* mutant background returned to normal levels by simultaneous deletion of either *nrf2* or deletion of both *mafG* and *mafF*.

When we examined *mafF::keap1* compound mutant forestomach in the hope of detecting an intermediate expression level of keratin 6, an unexpected result emerged, in that the level of keratin 6 mRNA in F0Kp0 pups was higher than in the Kp0 pups (Fig. 5*D*). One intriguing explanation for this result can be drawn from the unanticipated induction of *mafG* expression in the F0Kp0 forestomach (Fig. 5*E*). The regulatory mechanisms controlling *mafG* levels in the forestomach seem to be sensitive to the total amount of small Mafs, whereas those controlling *mafK* and *mafF* do not. MafG mRNA expression might be elevated because of compensatory mechanisms whose nature is unknown at present, but may involve autoregulation of a subset of the small Mafs. Consequently, more small Maf proteins are produced in the F0Kp0 forestomach, ending in higher expression of keratin 6 mRNA than in Kp0 mice. This result, although surprising, nonetheless further supports the contention that small Maf cooperatively activates Nrf2-dependent transcription *in vivo*.

Given the complexity of MARE-dependent gene regulation, germ-line mutagenesis and loss of function studies of each gene have proven to be a powerful approach to glean insight into the function of the molecules that interact with this site *in vivo*. Because small Maf proteins are capable of heterodimerizing with many bZip factors, including the CNC and Bach proteins, diminished small Maf abundance should be reflected by a functional defect in the activity of these multiple partner molecules. Megakaryocytic defects result as a consequence of defective p45 function or to a small Maf deficiency (32, 44–46). Similarly, aberrant constitutive induction of *heme oxygenase-1* can be attributed to a functional defect of Bach1 with insufficient small Maf partner molecules (47, 48). The other phenotypes observed in compound *small maf* mutant mice are red cell membrane abnormalities and a profound neurological disorder (34, 48), neither of which have been encountered in the analysis of Nrf2-deficient mice. This observation likely indicates

that the small Mafs also regulate batteries of genes that are not under Nrf2 regulatory influence. However, it does not exclude the possible involvement of Nrf2, because double or triple mutations including *nrf2* and other CNC transcription factor genes may recapitulate these phenotypes.

We have shown in this study that both *nrf2*-null mutant mice and small *maf* compound null mutant mice confer a similar rescue phenotype to *keap1*-null mutant mice, demonstrating that Nrf2-small Maf heterodimers play indispensable roles in keratinocytic gene expression. Considering the fact that excess small Mafs have been shown to repress transcription by forming inactive homodimers, keratinocytic overexpression of small Mafs would also be predicted to rescue *keap1*-null lethality. A recent study showed, using chromatin immunoprecipitation, that Nrf2 and small Maf are recruited to a MARE element in the mouse quinone reductase gene promoter when the gene is activated (43). This result is in very good agreement with the cooperative gene activation model executed by Nrf2 and small Maf that we propose here. In addition to oxidative stress-inducible genes, Nrf2 has been recognized as a critical regulator of other biological processes, including wound healing (49), endoplasmic reticulum stress response (40), inflammation resolution (50), and apoptosis (51). We suggest that the contribution of small Mafs to each of these Nrf2-dependent processes should be individually evaluated; some of the processes may depend on both Nrf2 and small Mafs, whereas the others may be independent of any small Maf contribution. Finally, the compound knockout–rescue approach exploited in the present study is an effective system for evaluating the *in vivo* contribution of test regulatory factors to Nrf2 activity, as long as mice deficient in these test factors are available. It would be interesting to apply this system to other candidate molecules that have been touted to be required for Nrf2 transcription activity, including other factors in the transcriptional machinery itself as well as specific signal transduction pathways.

We thank Ms. N. Kaneko and R. Kawai for technical assistance and Ms. K. Tong for critical reading. This work was supported in part by grants from the National Institutes of Health (CA80088 to J.D.E.), Exploratory Research for Advanced Technology (to M.Y.), the Ministry of Education, Science, Sports, and Technology (to H.M. and M.Y.), the Ministry of Health, Labor, and Welfare (to H.M. and M.Y.), the Japan Society for the Promotion of Science (to F.K.), Core Research for Evolutional Science and Technology (to H.M.), the Naito Foundation (to M.Y.), and the Special Coordination Fund for Promoting Science and Technology (to H.M.).

1. Motohashi, H., Shavit, J. A., Igarashi, K., Yamamoto, M. & Engel, J. D. (1997) *Nucleic Acids Res.* **25**, 2953–2959.
2. Kerppola, T. K. & Curran, T. (1994) *Oncogene* **9**, 3149–3158.
3. Kataoka, K., Noda, M. & Nishizawa, M. (1994) *Mol. Cell. Biol.* **14**, 700–712.
4. Kataoka, K., Igarashi, K., Itoh, K., Fujiwara, K. T., Noda, M., Yamamoto, M. & Nishizawa, M. (1995) *Mol. Cell. Biol.* **15**, 2180–2190.
5. Kawai, S., Goto, N., Kataoka, K., Saegusa, T., Shinno-Kohno, H. & Nishizawa, M. (1992) *Virology* **188**, 778–784.
6. Fujiwara, K. T., Kataoka, K. & Nishizawa, M. (1993) *Oncogene* **8**, 2371–2380.
7. Andrews, N. C., Erdjument-Bromage, H., Davidson, M. B., Tempst, P. & Orkin, S. H. (1993) *Nature* **362**, 722–728.
8. Igarashi, K., Kataoka, K., Itoh, K., Hayashi, N., Nishizawa, M. & Yamamoto, M. (1994) *Nature* **367**, 568–572.
9. Itoh, K., Igarashi, K., Hayashi, N., Nishizawa, M. & Yamamoto, M. (1995) *Mol. Cell. Biol.* **15**, 4184–4193.
10. Oyake, T., Itoh, K., Motohashi, H., Hayashi, N., Hoshino, H., Nishizawa, M., Yamamoto, M. & Igarashi, K. (1996) *Mol. Cell. Biol.* **16**, 6083–6095.
11. Marini, M. G., Chan, K., Casula, L., Kan, Y. W., Cao, A. & Moi, P. (1997) *J. Biol. Chem.* **272**, 16490–16497.
12. Onodera, K., Shavit, J. A., Motohashi, H., Katsuoka, F., Akasaka, J. E., Engel, J. D. & Yamamoto, M. (1999) *J. Biol. Chem.* **274**, 21162–21169.
13. Chan, J. Y., Han, X. L. & Kan, Y W. (1993) *Proc. Natl. Acad. Sci. USA* **90**, 11371–11375.
14. Kobayashi, A., Ito, E., Toki, T., Kogame, K., Takahashi, S., Igarashi, K., Hayashi, N. & Yamamoto, M. (1999) *J. Biol. Chem.* **274**, 6443–6452.
15. Kusunoki, H., Motohashi, H., Katsuoka, F., Morohashi, A., Yamamoto, M. & Tanaka, T. (2002) *Nat. Struct. Biol.* **9**, 252–256.
16. Itoh, K., Chiba, T., Takahashi, S., Ishii, T., Igarashi, K., Katoh, Y., Oyake, T., Hayashi, N., Satoh, K., Hatayama, I., *et al.* (1997) *Biochem. Biophys. Res. Commun.* **236**, 313–322.
17. Itoh, K., Wakabayashi, N., Katoh, Y., Ishii, T., Igarashi, K., Engel, J. D. & Yamamoto, M. (1999) *Genes Dev.* **13**, 76–86.
18. Enomoto, A., Itoh, K., Nagayoshi, E., Haruta, J., Kimura, T., O'Connor, T., Harada, T. & Yamamoto, M. (2001) *Toxicol. Sci.* **59**, 169–177.
19. Aoki, Y., Sato, H., Nishimura, N., Takahashi, S., Itoh, K. & Yamamoto, M. (2001) *Toxicol. Appl. Pharmacol.* **173**, 154–160.
20. Ramos-Gomez, M., Kwak, M. K., Dolan, P. M., Itoh, K., Yamamoto, M., Talalay, P. & Kensler, T. W. (2001) *Proc. Natl. Acad. Sci. USA* **98**, 3410–3415.
21. Wakabayashi, N., Itoh, K., Noda, S., Wakabayashi, J., Motohashi, H., Imakado, S., Kotsuji, T., Otsuka, F., Roop, D. R., Harada, T., *et al.* (2003) *Nat. Genet.* **35**, 238–245.
22. Dhakshinamoorthy, S. & Jaiswal, A. K. (2000) *J. Biol. Chem.* **275**, 40134–40141.
23. Gong, P., Hu, B., Stewart, D., Ellerbe, M., Figueroa, Y. G., Blank, V., Beckman, B. S. & Alam, J. (2001) *J. Biol. Chem.* **276**, 27018–27025.
24. Nguyen, T., Huang, H. C. & Pickett, C. B. (2000) *J. Biol. Chem.* **275**, 15466–15473.
25. Wild, A. C., Moinova, H. R. & Mulcahy, R. T. (1999) *J. Biol. Chem.* **274**, 33627–33636.
26. Alam, J., Stewart, D., Touchard, C, Boinapally, S., Choi, A. M. & Cook, J. L. (1999) *J. Biol. Chem.* **274**, 26071–26078.
27. Venugopal, R. & Jaiswal, A. K. (1998) *Oncogene* **17**, 3145–3156.
28. He, C. H., Gong, P., Hu, B., Stewart, D., Choi, M. E., Choi, A. M. & Alam, J. (2001) *J. Biol. Chem.* **276**, 20858–20865.
29. Hilberg, F., Aguzzi, A., Howells, N. & Wagner, E. F. (1993) *Nature* **365**, 179–181.
30. Tanaka, T., Tsujimura, T., Takeda, K., Sugihara, A., Maekawa, A., Terada, N., Yoshida, N. & Akira, S. (1998) *Genes Cells* **3**, 801–810.
31. Masuoka, H. C. & Townes, T. M. (2002) *Blood* **99**, 736–745.
32. Shavit, J. A., Motohashi, H., Onodera, K., Akasaka, J., Yamamoto, M. & Engel, J. D. (1998) *Genes Dev.* **12**, 2164–2174.
33. Katsuoka, F., Motohashi, H., Onodera, K., Suwabe, N., Engel, J. D. & Yamamoto, M. (2000) *EMBO J.* **19**, 2980–2991.
34. Onodera, K., Shavit, J. A., Motohashi, H., Yamamoto, M. & Engel, J. D. (2000) *EMBO J.* **19**, 1335–1345.
35. Stewart, D., Killeen, E., Naquin, R., Alam, S. & Alam, J. (2003) *J. Biol. Chem.* **278**, 2396–2402.
36. Nguyen, T., Sherratt, P. J., Huang, H. C., Yang, C. S. & Pickett, C. B. (2003) *J. Biol. Chem.* **278**, 4536–4541.
37. Itoh, K., Wakabayashi, N., Katoh, Y., Ishii, T., O'Connor, T. & Yamamoto, M. (2003) *Genes Cells* **8**, 379–391.
38. McMahon, M., Itoh, K., Yamamoto, M. & Hayes, J. D. (2003) *J. Biol. Chem.* **278**, 21592–21600.
39. Huang, H.-C., Nguyen, T. & Pickett, C. B. (2002) *J. Biol. Chem.* **277**, 42769–42774.
40. Cullinan, S. B., Zhang, D., Hannink, M., Arvisais, E., Kaufman, R. J. & Diehl, J. A. (2003) *Mol. Cell. Biol.* **23**, 7198–7209.
41. Ishii, T., Itoh, K., Takahashi, S., Sato, H., Yanagawa, T., Katoh, Y., Bannai, S. & Yamamoto, M. (2000) *J. Biol. Chem.* **275**, 16023–16029.
42. Kataoka, K., Handa, H. & Nishizawa, M. (2001) *J. Biol. Chem.* **276**, 34074–34081.
43. Nioi, P., McMahon, M., Itoh, K., Yamamoto, M. & Hayes, J. D. (2003) *Biochem. J.* **374**, 337–348.
44. Shivdasani, R. A., Rosenblatt, M. F., Zucker-Franklin, D., Jackson, C. W., Hunt, P., Saris, C. J. & Orkin, S. H. (1995) *Cell* **81**, 695–704.
45. Lecine, P., Blank, V. & Shivdasani, R. (1998) *J. Biol. Chem.* **273**, 7572–7578.
46. Motohashi, H., Katsuoka, F., Shavit, J. A., Engel, J. D. & Yamamoto, M. (2000) *Cell* **103**, 865–875.
47. Sun, J., Hoshino, H., Takaku, K., Nakajima, O., Muto, A., Suzuki, H., Tashiro, S., Takahashi, S., Shibahara, S., Alam, J., Taketo, M. M., Yamamoto, M. & Igarashi, K. (2002) *EMBO J.* **21**, 5216–5224.
48. Katsuoka, F., Motohashi, H., Tamagawa, Y., Kure, S., Igarashi, K., Engel, J. D. & Yamamoto, M. (2003) *Mol. Cell. Biol.* **23**, 1163–1174.
49. Braun, S., Hanselmann, C., Gassmann, M. G., auf dem Keller, U., Born-Berclaz, C., Chan, K., Kan, Y. W. & Werner, S. (2002) *Mol. Cell. Biol.* **22**, 5492–5505.
50. Itoh, K., Mochizuki, M., Ishii, Y., Ishii, T., Shibata, T., Kawamoto, Y., Kelly, V., Sekizawa, K., Uchida, K. & Yamamoto, M. (2004) *Mol. Cell. Biol.* **24**, 36–45.
51. Morito, N., Yoh, K., Itoh, K., Hirayama, A., Koyama, A., Yamamoto, M. & Takahashi, S. (2003) *Oncogene* **22**, 9275–9281.

*Kidney International, Vol. 65 (2004), pp. 1703–1713*

# Nrf2 deficiency improves autoimmune nephritis caused by the *fas* mutation *lpr*

**NAOKI MORITO, KEIGYOU YOH, AKI HIRAYAMA, KEN ITOH, MASATO NOSE, AKIO KOYAMA, MASAYUKI YAMAMOTO, and SATORU TAKAHASHI**

*Institute of Basic Medical Sciences, Institute of Clinical Medicine and Center for Tsukuba Advanced Research Alliance, University of Tsukuba, Tsukuba, Ibaraki, Japan; and Institute for Basic Medicine, Ehime University, Ehime, Japan*

**Nrf2 deficiency improves autoimmune nephritis caused by the *fas* mutation *lpr*.**

*Background.* Nrf2 is a basic leucine zipper transcriptional activator essential for the coordinate transcriptional induction of antioxidant and phase II drug metabolizing enzymes. We previously reported that Nrf2-deficient female mice develop lupus-like autoimmune nephritis (*Kidney Int* 60:1343–1353, 2001). The result suggested that *nrf2* is a possible candidate gene in determining susceptibility to autoimmune diseases. MRL/*lpr* mice, defective in Fas-mediated apoptosis, develop glomerulonephritis due to the production of autoantibodies.

*Methods.* To investigate the mechanism whereby Nrf2 contributes to the susceptibility to autoimmune diseases, we generated *nrf2 −/− lpr/lpr* mice.

*Results.* Unexpectedly, the lifespan of *nrf2 −/− lpr/lpr* female mice was markedly prolonged and these mice showed an improvement in nephritis compared to *nrf2+/+ lpr/lpr* female mice. Immunologic abnormalities and hypergammaglobulinemia were also alleviated in *nrf2−/− lpr/lpr* female mice. Furthermore, lymphadenopathy was suppressed as a result of increased apoptosis. To elucidate the molecular mechanism causing a stimulation of apoptosis, we analyzed the response made by *nrf2 −/− lpr/lpr* mice to death signals. We show that *nrf2−/− lpr/lpr* mice are sensitive to tumor necrosis factor-α (TNF-α)–mediated apoptosis. Since intracellular glutathione levels are decreased in Nrf2-deficient cells, it is probable that a prolonged depletion in glutathione levels leads to the enhancement in TNF-α–mediated apoptosis.

*Conclusion.* These results indicate that a deficiency in Nrf2 enhances TNF-α–mediated apoptosis which in-turn ameliorates the abnormal apoptotic response that arises from a mutation in the *lpr* gene. Therefore, Nrf2 deficiency acts as a suppressor of the autoimmune accelerating gene *lpr*.

Nrf2 [nuclear factor-erythroid 2 (NF-E2–related factor 2)] is a basic leucine zipper (b-Zip) transcriptional activator, originally identified as a protein capable of binding the NF-E2 promoter element [1, 2]. Nrf2 is essential for the coordinate transcriptional induction of antioxidant and phase II drug metabolizing enzymes through the antioxidant response element/electrophile response element (ARE/EpRE) [3, 4]. The ARE/EpRE sequence has been identified within the proximal regulatory sequences of antioxidant genes encoding glutathione S-transferase (GST) [5], NAD(P)H quinine oxidoreductase (NQO1) [6], heme oxygenase-1 (HO-1) [7], γ-glutamylcysteine synthetase [8], and cystine membrane transporter (system $Xc^-$) [9]. The ARE also regulates a wide range of metabolic responses to oxidative stress caused by reactive oxygen species (ROS) or electrophiles [9]. Understandably, targeted disruption of the *nrf2* gene in mice renders the animals sensitive to high levels of oxidative stress due to impairment in this stress response system [9–11].

We previously reported that aged Nrf2-deficient female mice presented with several immunopathologic features characteristic of human lupus, including splenomegaly, proteinuria, production of antinuclear antibodies, mesangial and capillary immune complex deposition with subsequent proliferative or crescentic change within glomeruli, and, eventually, renal failure and death [12]. These findings indicate a role for oxidative stress in the development of lupus, and also point to *nrf2* as a possible candidate gene in determining susceptibility to autoimmune diseases. A number of lupus models and mouse strains have been established and studied extensively with respect to disease pathogenesis, including MRL/Mp-*lpr/lpr* (MRL/*lpr*) [13], BXSB/MpJ*Yaa* [13], and NZB/NZW F1 [14, 15]. However, linkage of the *nrf2* gene to any of these lupus strains has not been described previously. MRL/*lpr* mice spontaneously develop lymphadenopathy and an autoimmune disorder characterized by immune complex glomerulonephritis, arthritis, vasculitis, and antinuclear antibodies [13]. The predominant cell type that occupies the lymphoid organ are phenotypically double negative ($CD4^-CD8^-$) with respect to T-cell surface markers. These cells also possess the B220 cell surface marker usually restricted to B cells. The

**Key words:** Nrf2, Fas, TNF-α, glutathione, apoptosis, oxidative stress.

Received for publication January 22, 2003
and in revised form September 11, 2003, and November 5, 2003
Accepted for publication December 1, 2003

double negative T cells also display hallmarks of mature T lymphocytes, including CD3 and the αβ-TCR [13]. The genetic defect that leads to lymphoproliferation *(lpr)* is a mutation in the gene coding Fas [16], a cell surface molecule that belongs to the tumor necrosis factor (TNF) receptor gene family. The development of lymphadenopathy and of autoimmune disease in *lpr* mice has been attributed to a defect in Fas-mediated apoptosis causing a failure in the activation-induced cell death of activated T cells [16, 17]. Thus, the *lpr* gene is believed to be the fundamental molecular abnormality in MRL/*lpr* mice. However, the spectrum of autoimmune manifestations is greatly affected by the host genetic background. For example, when the *lpr* is crossed on to the MRL/Mp strain, the disease is markedly accelerated, and most mice die by 6 months of age [18]. Whereas, MRL/*lpr*, *lpr* congenic mice of the C3H/HeJ, AKR or C57BL/6 background rarely develop nephritis or vasculitis [19–21]. These results indicate that the development of autoimmune diseases in MRL/*lpr* mice requires both an accelerating gene (*lpr*) and susceptibility genes (genes specific to the genetic background).

To further define the mechanism whereby Nrf2 determines the susceptibility to autoimmune diseases, we generated *nrf2−/− lpr/lpr* female mice and estimated the survival rate and the development of glomerulonephritis.

Unexpectedly, *nrf2−/− lpr/lpr* female mice had a significantly longer lifespan and less severe nephritis than *nrf2+/+ lpr/lpr* female mice. Detailed analyses revealed that, in *lpr* mice, a deficiency in Nrf2 enhanced the sensitivity of TNF-α–mediated apoptosis and suppressed the autoimmune acceleration effect of the *lpr* gene. These results demonstrate that Nrf2 deficiency may act as suppressor of the autoimmune accelerating gene *lpr*, instead of being a susceptibility gene in these mice.

## METHODS

### Generation of *nrf2* mutant *lpr* mice

The generation of Nrf2-deficient mice was previously described [4]. Genotypes of homozygous wild-type and Nrf2-deficient mice were confirmed by polymerase chain reaction (PCR) amplification of genomic DNA isolated from tails. PCR amplification was carried out by using three different primers, 5′-TGGACGGGACTATTGAA GGCTG-3′ (sense for both genotypes), 5′-CGCCTTTT CAGTAGATGGAGG-3′ (antisense for wild-type), and 5′-GCGGATTGACCGTAATGGGATAGG-3′ (antisense for LacZ). MRL/*lpr* mice were obtained from Japan SLC (Shizuoka, Japan). Intercrossing Nrf2-deficient mice with an ICR background and MRL/*lpr* mice generated *nrf2−/− lpr/lpr* mice and control *nrf2+/+ lpr/lpr* mice. The present study utilized female mice from the same litters. Mice were maintained in the Laboratory Animal Resource Center. All experiments were performed according to the Guide for the Care and Use of Laboratory Animals in University of Tsukuba.

### Measurement of urinary protein, serum creatinine, and blood urea nitrogen

The urine of each mouse was collected in individual metabolic cages over a 24-hour period from *nrf2−/− lpr/lpr* and *nrf2+/+ lpr/lpr* 20-week-old female mice. The amount of proteinuria was assessed by measuring the turbidity obtained with 3% sulphosalicylic acid. Protein values more than 2 mg/24 hours were considered abnormal. The concentration of serum creatinine and blood urea nitrogen (BUN) were measured by an automated analyzer for routine laboratory tests (Dry-Chem 3500) (Fuji Film, Inc., Tokyo, Japan).

### Histopathologic analysis of renal tissues

Each mouse was bled while under ether anesthesia. Sera were stored at −80°C until use. At autopsy, organs were fixed with 10% formalin in 0.01 mol/L phosphate buffer (pH 7.2) and embedded in paraffin. Sections were stained with hematoxylin and eosin for histopathologic examination under light microscopy. For semiquantitative histologic analysis, more than 20 glomeruli from each kidney section were examined. The degree of glomerular lesion was estimated using a scale of 0 to 3 based on the severity and extent of histopathologic changes, as described previously [19]. The index of glomerular lesion is the mean value of more than 20 observed glomeruli. Sections frozen for immunofluorescent analysis were stained using fluorescein isothiocyanate (FITC)-labeled antimouse IgG, IgG1, IgG2a, IgG3, IgM, and C3 (ICN Pharmaceuticals, Inc., Aurora, OH, USA). Quantitative estimation of immunofluorescent staining was performed using ImageJ (National Institutes of Health, Bethesda, MD, USA). Relative fluorescent intensity was described as the mean fluorescent intensity of *nrf2+/+ lpr/lpr* mice equals 1.0.

### Immunohistochemical examination

Kidneys that were to be used for immunoperoxidase staining were snap-frozen in optimal cutting temperature (OCT) (Miles Scientific, Naperville, IL, USA) and stored at −80°C. We identified macrophage (F4/80), CD4-, CD8-, and B220-positive cells using monoclonal antibodies as described by Iwata et al [22]. Anti-CD4, CD8, and B220 antibodies were purchased from BD Biosciences (San Jose, CA, USA) and anti-F4/80 antibody from Serotec (Oxford, UK). These cells were identified by avidin-biotin complex immunoperoxidase technique using Histofine Kit (Nichirei, Tokyo, Japan). We counted macrophage, CD4-, CD8-, and B220-positive cells in periglomerular areas of 10 randomly selected glomeruli

and have expressed the results as cells/glomerulus. Interstitial CD4-, CD8-positive T cells and B220-positive cells were counted in 10 randomly selected fields of cortical interstitium using a light microscope (magnification, ×400) and described as/fields.

### Cytokine expression

We evaluated renal colony stimulating factor 1 (CSF-1), monocyte chemoattractant protein 1 (MCP-1), TNF-α, transforming growth factor 1 (TGF-β1) and interferon γ (IFN-γ) transcripts by reverse transcription-polymerase chain reaction (RT-PCR) method. Total RNA was extracted from the kidney using TRIzol (Invitrogen, Carlsbad, CA, USA). RT was performed using the SuperScript First-Stranded Synthesis System for RT-PCR (Invitrogen). The complementary DNA product was amplified by PCR. Primers (CSF-1, 5′ primer AAA GCCACTCTTGGGGCATT, 3′ primer TCGATGGCT CCACTTCC; MCP-1, 5′ primer AGCAGGTGTCCCA AAGAAGC, 3′ primer ACAAAGTTTACCCATTCA TC; TNF-α 5′ primer AGGTTCTCTTCAAGGGAC AA, 3′ primer TCACAGAGCAATGACTCCAA; TGF-β1, 5′ primer GGACCTGGGTTGGAAGTGGA, 3′ primer GCGACCCACGTAGTAGACGA; IFN-γ, 5′ primer CAAGTGGCATAGATGTGGAA, 3′ primer G TTGTTGACCTCAAACTTGG; GAPDH, 5′ primer CCCCTTCATTGACCTCAACTACATGG, 3′ primer GCCTGCTTCACCACCTTCTTGATGTC) were used for PCR. The housekeeping gene glyceraldehyde-3-phosphate dehydrogenase (GAPDH) was used for PCR controls.

### Total glutathione (GSH) level of kidneys

Kidneys from *nrf2−/− lpr/lpr* and *nrf2+/+ lpr/lpr* 20-week-old female mice were homogenized and suspended in 5% sulfosalicylic acid. Subsequently, total GSH level was measured by an enzyme recycling method using the Total Glutathione Quantification Kit (Dojindo, Kumamoto, Japan).

### Measurement of serum immunoglobulin

Serum immunoglobulin was determined by enzyme-linked immunosorbent assay (ELISA) as previously described [12]. Briefly, Nunc-Immunoplates (Nunc A/S, Roskilde, Denmark) were coated with goat antimouse immunoglobulin (ICN Pharmaceuticals, Inc.). The plates were kept at room temperature for 1 hour and were then washed with 0.1 mol/L phosphate-buffered saline (PBS). After washing, the plates were blocked with 0.5% bovine serum albumin (BSA) in a PBS solution. Serial dilutions of test serum samples were applied and incubated at room temperature for 1 hour. After washing with PBS, the plates were treated with alkaline phosphatase-conjugated goat antimouse IgM, IgG, IgG1,and IgG2a (Sigma Chemical Co., St. Louis, MO, USA) at room temperature for 1 hour. After additional washes, alkaline phosphatase substrate (Sigma Chemical Co.) solution was added and allowed to develop. Absorption at 405 nm was measured using an immuno-plate reader (BenchMark) (Bio-Rad, Hercules, CA, USA). In order to measure IgG3 levels, single radial immunodiffusion (SRID) was performed. One percent agalose gels in 0.1 mol/L PBS, pH7.2, which contained anti-Ig isotype serum (rabbit antimouse IgG3), was purchased from Miles Laboratories Inc. (Elkhart, IN, USA) were prepared and spread on a glass plate. Samples (4 μL) were applied to punched holes of 1.5 mm in diameter and the slides were incubated at room temperature for 48 hours. Precipitation rings were measured after staining with AminoBlock 10B.

### Anti-double-stranded DNA antibody assay

ELISA was used to determine the titer of anti-double stranded DNA antibody in sera as described previously [19]. Nunc-Immunoplates were coated with protamine sulfate (Sigma Chemical Co.). Subsequently, a solution of double-stranded DNA was added to the plates. The double-standed DNA was prepared from calf thymus DNA treated with S1 nuclease (Sigma Chemical Co.) to eliminate single-stranded DNA according to the published method [23]. The plates were kept at 4°C overnight and then washed with PBS. Afterward, the plates were blocked with 0.5% BSA in PBS solution. Serial dilutions of test serum samples were added and incubated at room temperature for 1 hour. After washing with PBS, the plate was treated with alkaline phosphatase-conjugated goat antimouse IgG (Sigma Chemical Co.) and processed as described previously in this article. The titer of anti-double-stranded DNA antibodies in pooled sera from four 20-week-old MRL/*lpr* female mice was set at 100 units.

### Lymphadenopathy scoring

Arbitrary clinical scoring of lymphnodes was assigned by an observer blinded to group identities, using a scale of 0–4 (0 = none; 1 = a single node anywhere; 2 = bilateral axillary; 3 = femoral, or cervical nodes; and 4 = massive generalized adenopathy) [24].

### Fluorescence-activated cell sorter (FACS) analysis

Single-cell suspensions were prepared from the lymphnodes of each mouse and blocked with anti-FcγR antibody (2.4G2) for 10 minutes on ice to inhibit the interaction of staining reagents with the cell surface. Multicolor flow cytometry analysis was performed using LSR and Cellquest software (Becton Dickinson,

Franklin Lakes, NJ, USA) on viable cells as determined by forward light scatter intensity and propidium iodide exclusion. The following phycoerythrin (PE), FITC, or peridinin chlorophyll protein (perCP)-labeled monoclonal antibodies were used: anti-CD4-PE, anti-CD8-FITC, anti-CD3-perCP (BD Biosciences) and anti F4/80-PE (Serotec). Bilateral cervical and axillary lymphnodes were obtained from *nrf2−/− lpr/lpr* and *nrf2+/+ lpr/lpr* mice. Total cell numbers of each lymphocytes and macrophages were counted.

### Terminal deoxynucleotidyl transferase (TdT) nick end-labeling (TUNEL) assay

Apoptotic cells were estimated by the TUNEL assay, which relies on incorporation of labeled deoxyuridine triposphate (dUTP) at sites of DNA breaks. For the TUNEL procedure, all reagents, including buffer, were part of a kit (In situ Takara Apoptosis Kit; Takara, Inc., Otsu, Japan). Procedures were carried out according to the manufacturer's instructions. Apoptosis was examined in 5 μm thick sections of the spleens, kidneys, and livers of *nrf2−/− lpr/lpr* and *nrf2+/+ lpr/lpr* mice. For quantitative histologic analysis, the degree of apoptosis was estimated using a scale based on the mean number of TUNEL-positive cells per 20 microscopic fields, or per field (magnification, ×400).

### Induction of splenocyte apoptosis by TNF-α

Splenocytes were isolated from 8-week-old *nrf2−/− lpr/lpr* and *nrf2+/+ lpr/lpr* mice. The cells were washed in Dulbecco's modified Eagle's medium (DMEM) supplemented with 10% heat-inactivated fetal bovine serum (FBS), 0.5 mmol/L 2-mercaptoethanol, 2 mmol/L glutamine, 1 mmol/L *N*-2-hydroxyethylpiperazine-*N'*−2-ethanesulfonic acid (HEPES) (pH 7.4) and antibiotics (all from Invitrogen Inc.). The cells were again washed in medium before use in subsequent tissue culture experiments. The cells ($1 \times 10^6$/mL) were incubated with various concentrations of TNF-α for 12 hours. TNF-α was purchased from BD Biosciences. Cell viability was determined by trypan blue exclusion. The cells were preincubated with glutathione ethyl monoester (GSH-OEt) (2 mmol/L for 15 to 20 minutes) to increase the intracellular pool of GSH. GSH-OEt was obtained from Wako (Osaka, Japan).

### Hepatocellular apoptosis induction by administration of anti-Fas antibody and TNF-α in mice

Agonistic antimouse Fas antibody (Jo-2) (BD Biosciences) (2 mg/mouse) was administered to 20-week-old female mice intraperitoneally in sterile saline solution. Human recombinant TNF-α (BD Biosciences) (0.5mg/mouse) was also administered intraperitoneally. To increase the TNF-α sensitivity, D-galactosamine hydrochloride (GalN) (Nacalai Tesque, Tokyo, Japan) was preinjected intravenously 30 minutes before TNF-α injection. To assess the importance of the intracellular GSH level, GSH-OEt (20 mg/mouse) was preinjected intravenously 2 hours before TNF-α injection and the same experiments performed. Hepatocellular injury was monitored biochemically by measuring serum alanine aminotransferase (ALT) activity using an automated analyzer (Dry-Chem 3500) (Fuji Film). At the end of the experimental period mice were sacrificed for necropsy. The liver was excised, fixed with 10% buffered formalin, sectioned at a thickness of 5 μm, and stained with hematoxylin and eosin for examination by light microscope.

### Statistical analysis

Results were expressed as means ± SEM. Multiple data comparisons were performed using the one-way analysis of variance (ANOVA) routinely with the Bonferroni correction. Significant differences between the groups of mice were analyzed using the Wilcoxon test for paired samples, and $P$ values less than 0.05 were considered statistically significant. Comparisons of survival rate were done by the Kaplan-Meier method.

## RESULTS

### Survival rate

*nrf2−/− lpr/lpr* female mice had a markedly prolonged lifespan with 50% of the mice having survival times twice as long as *nrf2+/+ lpr/lpr* female mice (Fig. 1). The 50% survival weeks of *nrf2−/− lpr/lpr* female mice were 45.4 ± 2.2 weeks in comparison to 23.2 ± 6.1 weeks for the *nrf2+/+ lpr/lpr* female mice. The 50% survival weeks of MRL/*lpr* mice was 6 months [18], which was almost the same as that of *nrf2+/+ lpr/lpr* mice.

### Renal function and urinary protein

MRL/*lpr* mice are known to die from renal failure caused by autoimmune kidney disease [13]. We evaluated renal function in *nrf2−/− lpr/lpr* mice by measuring serum creatinine and BUN, as an index of renal function, in a time series experiment. The levels of serum creatinine and BUN were decreased in *nrf2−/− lpr/lpr* mice compared to *nrf2+/+ lpr/lpr* mice at 20 weeks old, but only significantly in the case of BUN levels. We also performed other studies, including urinary protein analysis, at 20 weeks of age (Table 1). The urinary protein levels of *nrf2−/− lpr/lpr* female mice were significantly lower than that of *nrf2+/+ lpr/lpr* female mice at 20 weeks of age.

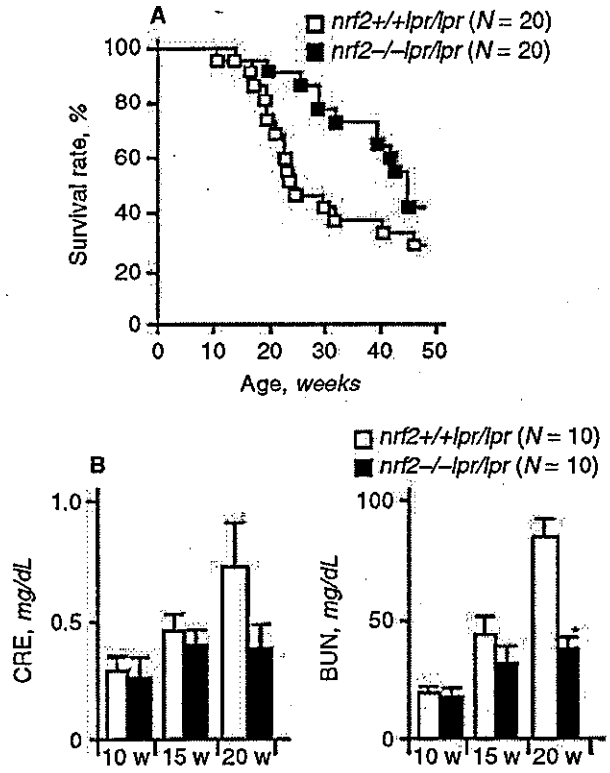


**Fig. 1. Survival rate and renal function of *lpr* female mice.** (*A*) Survival rate of *nrf2−/− lpr/lpr* ($N = 20$) and *nrf2+/+ lpr/lpr* ($N = 20$) female mice using Kaplan-Meier method. The difference in survival rate between *nrf2−/− lpr/lpr* and *nrf2+/+ lpr/lpr* mice was significant ($P < 0.05$). (*B*) Serum creatinine (CRE) and blood urea nitrogen (BUN) were decreased in *nrf2−/− lpr/lpr* mice ($N = 10$) compared to *nrf2+/+ lpr/lpr* mice ($N = 10$) at 20 weeks old, but only BUN showed a significant decrease (*$P < 0.05$) (serum creatinine, $P = 0.08$). Each bar represents the mean± SEM.

**Table 1.** Clinical and serologic manifestations in *nrf2 −/− lpr/lpr* and *nrf2 +/+ lpr/lpr* female mice at 20 weeks of age[a]

| | *nrf2 −/− lpr/lpr* | *N* | *nrf2 +/+ lpr/lpr* | *N* | *P* value |
|---|---|---|---|---|---|
| Urinary protein *mg/day* | 1.2 ± 0.3 | 15 | 3.6 ± 1.0 | 16 | <0.05 |
| IgM *mg/dL* | 469.4 ± 52.1 | 10 | 624.9 ± 111.2 | 10 | NS |
| IgG *mg/dL* | 2821.5 ± 353.1 | 10 | 8526.1 ± 788.9 | 10 | <0.05 |
| IgG1 *mg/dL* | 199.8 ± 35.1 | 10 | 524.3 ± 88.4 | 10 | <0.05 |
| IgG2a *mg/dL* | 1815.2 ± 318.4 | 10 | 6226.7 ± 1475.0 | 10 | <0.05 |
| IgG3 *mg/dL* | 651.2 ± 86.3 | 10 | 913.4 ± 104.2 | 10 | NS |
| Anti-dsDNA IgG *units* | 31.5 ± 10.3 | 10 | 103.3 ± 22.7 | 10 | <0.05 |
| Lymphadenopathy score[b] | 0.9 ± 0.3 | 20 | 1.5 ± 0.5 | 20 | <0.05 |

ds DNA is double-stranded DNA.
[a]Results are shown as means ± SEM; [b]Using a scale of 0 to 4 described in the **Methods** section.

## Histologic analysis

Renal histopathologic studies were performed in *nrf2−/− lpr/lpr* and *nrf2+/+ lpr/lpr* female mice at 20 weeks of age. In *nrf2+/+ lpr/lpr* female mice, glomerulonephritis with inflammation, sclerosis, and crescent formation were observed (Fig. 2A). By contrast, glomerular lesions were improved in *nrf2−/− lpr/lpr* female mice (Fig. 2B). The average of indices of glomerular lesions (as described in the **Methods** section) in *nrf2+/+ lpr/lpr* and *nrf2−/− lpr/lpr* female mice were 2.8 ± 0.3 ($N = 10$) and 2.0 ± 0.2 ($N = 10$), respectively ($P < 0.05$). IgG, IgM, and C3 deposits were observed by immunofluorescence staining in the kidney of both *nrf2−/− lpr/lpr* and *nrf2+/+ lpr/lpr* mice. IgG and C3 deposits in the mesangial regions and the capillary walls of glomeruli were decreased in *nrf2−/− lpr/lpr mice* compared to *nrf2+/+ lpr/lpr* mice ($P < 0.05$). From the isotype staining of IgG, IgG2a and IgG3 deposits were found to be decreased in *nrf2−/− lpr/lpr mice* compared to *nrf2+/+ lpr/lpr* mice, significantly ($P < 0.05$) (Fig. 2C and D).

## Immunohistochemical examination

Abnormal renal function in MRL/*lpr* mice consists of leukocyte infiltration, including macrophage, CD4 and CD8 T cells, and B220-positive cells [22]. We evaluated the numbers of these infiltrates in the glomeruli and interstitium *nrf2−/− lpr/lpr* kidneys at 20 weeks old. The numbers of macrophage (F4/80), CD4, CD8-positive T cells, and B220-positive cells were significantly reduced in *nrf2−/− lpr/lpr* kidneys compared with *nrf2+/+ lpr/lpr* kidneys (Fig. 3A and B). It has been reported that B220-positive cells in the kidney are unique double negative T cells and are not B cells in MRL/*lpr* mice [25, 26]. This result suggests that the reduction in numbers of macrophages, CD4, CD8-positive and double-negative T cells would lead to an improvement of kidney disease in *nrf2−/− lpr/lpr* mice.

## Influence of *nrf2 −/−* on the level of key cytokines

It was previously reported that CSF-1, MCP-1, TNF-α, TGF-β1, and IFN-γ transcripts are up-regulated with the onset of renal injury in MRL/*lpr* mice and are a causative factor in the progression of autoimmune kidney disease [27–31]. So we determined these cytokines transcript levels by RT-PCR method. In *nrf2−/− lpr/lpr* kidneys, CSF-1, MCP-1, TNF-α, TGF-β1, and IFN-γ transcripts were reduced compared to *nrf2+/+ lpr/lpr* kidneys. (Fig. 3C).

## Level of GSH in renal tissue

It has previously been described that various antioxidant and detoxification enzymes which are subject to Nrf2 regulation are reduced in the liver and macrophages of Nrf2-deficient mice [5–9]. As a consequence, Nrf2 deficiency may lead to high levels of oxidative stress and a depletion of GSH synthetic enzymes. We hypothesized that a reduction in GSH in renal tissue could influence the pathogenesis of autoimmune kidney disease. Therefore we measured renal GSH levels in *nrf2−/− lpr/lpr*

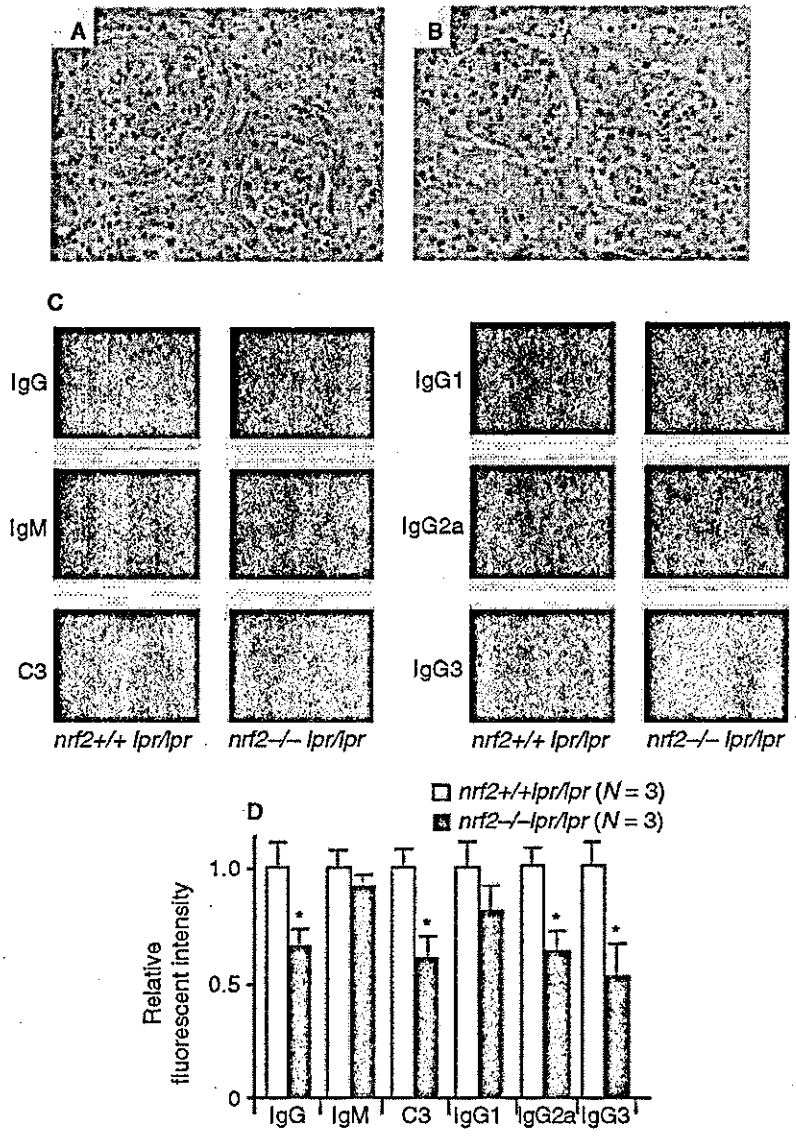


**Fig. 2. Histopathologic analysis of renal tissues in *nrf2−/− lpr/lpr* mice.** Renal section from an *nrf2−/− lpr/lpr* 20-week-old female mouse (*B*) showed the improvement of glomerular lesions compared to an age-matched *nrf2 +/+ lpr/lpr* mouse (*A*) (×100, hematoxylin and eosin stain). Immunofluorescent staining of IgG, IgM, C3, IgG1, IgG2a, and IgG3 (*C*). IgG, IgG2a, IgG3, and C3 deposits in the mesangial regions and the capillary walls of glomeruli were decreased in *nrf2−/− lpr/lpr* mice compared to *nrf2+/+ lpr/lpr* mice (×400). Quantitative analysis of immunofluorescent stainig revealed IgG, IgG2a, IgG3, and C3 deposits were significantly decreased in *nrf2−/− lpr/lpr* mice (*D*) (*$P < 0.05$). Each bar represents the mean ± SEM.

mice. Renal GSH was significantly reduced in *nrf2−/− lpr/lpr* mice compared to *nrf2+/+ lpr/lpr* mice (Fig. 3D).

### Serum immunoglobulin and anti-double-stranded DNA antibodies

To evaluate immunologic abnormalities, the serum immunoglobulins in *nrf2−/− lpr/lpr* and *nrf2+/+ lpr/lpr* female mice at 20 weeks of age were measured. There was no significant difference in serum IgM levels between *nrf2−/− lpr/lpr* and *nrf2+/+ lpr/lpr* female mice (Table 1). Serum IgG levels of *nrf2−/− lpr/lpr* were lower than those of *nrf2+/+ lpr/lpr* female mice. Serum immunoglobulin levels of *nrf2+/+ lpr/lpr* female mice were almost comparable to those of MRL/*lpr* female mice as previously described [32]. The levels of IgG, IgG1, and IgG2a were also decreased in *nrf2−/− lpr/lpr* female mice compared to *nrf2+/+ lpr/lpr* female mice (Table 1). Serum IgG3 level in *nrf2−/− lpr/lpr* was also lower than *nrf2+/+ lpr/lpr* mice, but not significantly. There was not a significant difference in serum IgG3 level between *nrf2−/− lpr/lpr* and *nrf2+/+ lpr/lpr* mice. However, in immunofluorescence staining, IgG3 deposition was decreased in *nrf2−/− lpr/lpr* mice compared to *nrf2+/+ lpr/lpr* mice. This result suggests IgG3 is one of the major factors responsible for the development of glomerulonephritis in *lpr/lpr* mice. The production of anti-double-stranded DNA autoantibody was significantly reduced in *nrf2−/− lpr/lpr* female mice when compared to *nrf2+/+ lpr/lpr* female mice ($P < 0.05$) (Table 1). Since the amount of anti-double-stranded DNA autoantibody in pooled sera from 20-week-old MRL/*lpr* female mice was set